Natural Convection Heat Transfer From an Isothermal Plate

Aubrey G. Jaffer
e-mail: agj@alum.mit.edu

Abstract

Using boundary-layer theory, natural convection heat transfer formulas which are accurate over a wide range of Rayleigh numbers (Ra) were developed in the 1970s and 1980s for vertical and downward-facing plates. A comprehensive formula for upward-facing plates remained unsolved because they do not form conventional boundary-layers.

From the thermodynamic constraints on heat-engine efficiency, the novel approach presented here derives formulas for natural convection heat transfer from isothermal plates. The union of four peer-reviewed data-sets spanning $1 < Ra < 10^{12}$ has 5.4% root-mean-squared relative error (RMSRE) from the new upward-facing heat transfer formula.

Applied to downward-facing plates, this novel approach outperforms the Schulenberg (1985) formula's 4.6% RMSRE with 3.8% on four peer-reviewed data-sets spanning $10^6 < Ra < 10^{12}$.

The introduction of the harmonic mean as the characteristic length metric for vertical and downward-facing plates extends those rectangular plate formulas to other convex shapes, achieving 3.8% RMSRE on vertical disk convection from Hassani and Hollands (1987) and 3.2% from Kobus and Wedekind (1995).

This research did not receive any specific grant from funding agencies in the public, commercial, or not-for-profit sectors.

Table of Contents

1. Introduction

Natural convection is the flow caused by nonuniform density in a fluid. It is a fundamental process with applications from engineering to geophysics.

When a stationary, immersed object changes temperature, nearby fluid can change density as it warms or cools. Under the influence of gravity, density changes cause fluid to flow. The rates of fluid flow and heat transfer from the object grow until reaching a plateau. This investigation seeks to predict the overall steady-state heat transfer rate from an external, flat, isothermal surface inclined at any angle in a Newtonian fluid.

An "external" plate is one that fluid can flow around freely, especially horizontally. If enclosed, the enclosure must have dimensions much larger than the heated or cooled surface. Natural convection in an enclosure of size comparable to the heated or cooled surface can organize into cells of Rayleigh-Bénard convection, which is not treated here.

The characteristic length L is the length scale of a physical system. For many heat transfer processes, it is the volume-to-surface-area or area-to-perimeter ratio of the heated or cooled object. There are several characteristic length metrics used for natural convection, some of which are valid only for convex objects. This investigation focuses on flat plates with convex perimeters.

1.1 Flow Topologies.

There are three topologies of convective flow from external, convex plates.

For a horizontal plate with heated upper face, streamlines photographs in Fujii and Imura [1] show natural convection pulling fluid horizontally from above the plate's perimeter into a rising central plume. Figure 1, below, is a diagram of this upward-facing convection. Horizontal flow is nearly absent at the elevation of the dashed line.

Kitamura, Mitsuishi, Suzuki, and Kimura [2] shows top-views of plumes from heated rectangular plates with aspect ratios between 1:1 and 8:1. The plates with high aspect ratios have a plume over the plate's mid-line parallel to the longer sides, but not as long.

The streamlines photograph of a vertical plate in Fujii and Imura [1] shows fluid being pulled horizontally before rising into a plume along the vertical plate.

Modeled on a streamlines photograph in Aihara, Yamada, and Endö [3], Figure 2 is a flow diagram for a horizontal plate with heated lower face. Unheated fluid below the plate flows horizontally inward. It rises a short distance, flows outward closely below the plate, and flows upward upon reaching the plate edge.

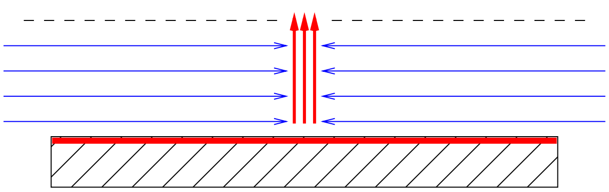

Figure 1 flow above a heated plate

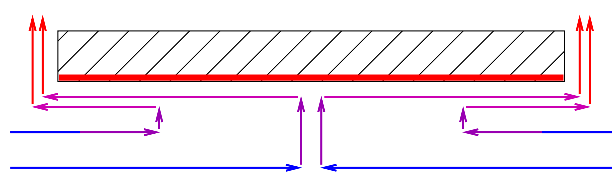

Figure 2 flow below a heated plate

There is a symmetry in external natural convection; a cooled plate induces downward flow instead of upward flow. Flow from a cooled upper face is the mirror image of flow from a heated lower face. Flow from a cooled lower face is the mirror image of flow from a heated upper face.

Sublimation from an upper face is downward convection when the dissolved sublimate is denser than the fluid. The rest of this investigation assumes a heated plate.

An important aspect of all three flow topologies is that fluid is pulled horizontally before being heated by the plate. Pulling horizontally expends less energy than pulling vertically because the latter does work against the gravitational force. Inadequate horizontal clearance around a plate can obstruct flow and reduce convection and heat transfer.

1.2 Fluid Mechanics.

In fluid mechanics, the convective heat transfer rate is represented by the average Nusselt number ($\overline{Nu}$). The Rayleigh number (Ra) is the impetus to flow due to temperature difference and gravity. A fluid's Prandtl number (Pr) is its momentum diffusivity per thermal diffusivity ratio. These three "variable groups" are dimensionless (measurement units of the constituent variables cancel each other).

The characteristic length L scales $\overline{Nu}$; Ra is scaled by L^3; Pr is independent of L.

Formulas for heat transfer can apply to mass transfer via analogous variable groups, such as Schmidt number (Sc) and Pr. Figure 3 has Sherwood number ($\overline{Sh}$) instead of $\overline{Nu}$ on its vertical axis.

1.3 **Turbulence Versus Laminar Flow.** Previous investigations [1, 2, 4, 5] assumed that natural convection heat transfer formulas would differ substantially when the convection was turbulent versus laminar. For their upward-facing plate, Lloyd and Moran [4] reported that the transition from laminar to turbulent flow occurred at $Ra \approx 8 \times 10^6$. The straight line segments they fitted to their data at greater and lesser Ra were disjoint at $Ra = 8 \times 10^6$. However, with their fit lines removed, if $Ra \approx 8 \times 10^6$ represents a discontinuity, then it is one of several, and subsumed within the scatter of their measurements in Figure 3.

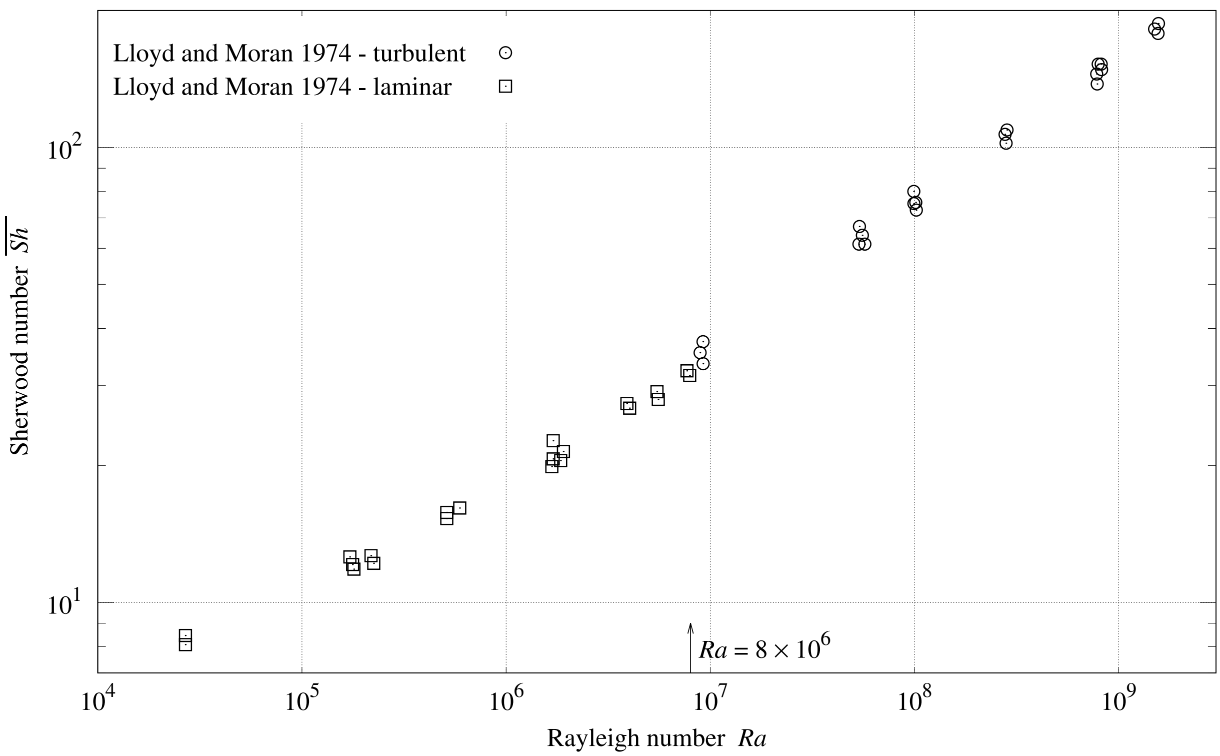

Figure 3 upward convection mass transfer from horizontal plate

About their measurements of vertical and downward tilted plates, Fujii and Imura [1] wrote:

> "Though the boundary layer was not always laminar near the trailing edge for large $Gr\,Pr$ [$= Ra$] values, no influence of the flow regime on the data shown in [their] Fig. 6 is appreciable."

Churchill and Chu [5] concludes that one of its equations

> "...based on the model of Churchill and Usagi [6] provides a good representation for the mean heat transfer for free convection from an isothermal vertical plate over a complete range of Ra and Pr from 0 to ∞ even though it fails to indicate a discrete transition from laminar to turbulent flow."

The lack of a significant transition between the rates of (mean) heat transfer in laminar and turbulent natural convection indicates that some more basic principle organizes natural convection.

1.4 **Thermodynamics.** The fundamental laws of thermodynamics make no distinction between laminar and turbulent flows. Considering a small object inside a very tall column of fluid as a closed system, natural convection is a heat-engine which converts the temperature difference between the object and fluid into flow of that fluid. The heated object is the heat source; fluid far above the object is the heat sink.

System-wide thermodynamic constraints cannot be enforced locally, requiring a radical departure from boundary-layer analysis (which is based on local flow solutions of the Navier-Stokes equations). This investigation solves algebraic equations in terms of average fluid velocity, heat conduction, and power flux.

2. Materials and Methods

2.1 **Not Empirical.** Empirical theories derive their coefficients from measurements, inheriting the uncertainties from those measurements. Theories developed from first principles derive their coefficients mathematically. For example, the Blasius model of laminar flow coefficient 0.3320+ is the solution of a differential equation (Lienhard and Lienhard [7]). Another example is the heat conduction shape factor for one face of a disk, which is exactly twice its diameter. The present theory derives from first principles; it is not empirical. [1] Each equation term is tied to an aspect of the plate geometry, orientation, and flow diagram.

This investigation tests its theory on prior works' measurement data with as wide a range of Ra and Pr as possible. Few of the cited studies provided estimated measurement uncertainties. Root-mean-squared relative error (RMSRE), introduced in Section 8, provides an objective, quantitative evaluation of each data set versus the theory.

2.2 **Detail.** Were this theory derived using the usual fluid-mechanics techniques, derivation detail would be unnecessary. However, this powerful new methodology is unlike those techniques. The first derivations provide more detail to enable readers to adapt the present methodology to other fluid mechanics problems.

Table 1 sources of measurements

Source	**Description**	**Fluid**	$Pr\|Sc$	**Face**	$Ra \geq$	$Ra \leq$	$\pm$
[1] Fujii & Imura	5×10 cm	water	5.0	up	5.7×10^6	1.3×10^9	
[1] Fujii & Imura	30×15 cm	water	5.0	up	4.1×10^9	4.8×10^{11}	
[8] Goldstein et al.	sublimation	air	2.50	up	1.6×10^0	6.2×10^3	
[4] Lloyd & Moran	electrochemical	H_2SO_4	2200	up	2.6×10^4	1.6×10^9	5%
[5] Churchill & Chu	Cheesewright	air	0.70	vertical	7.0×10^3	1.5×10^9	
[5] Churchill & Chu	Jakob	air	0.70	vertical	2.1×10^7	1.0×10^{12}	
[5] Churchill & Chu	King	air	0.70	vertical	3.6×10^3	1.5×10^8	
[5] Churchill & Chu	Saunders	mercury	0.024	vertical	2.7×10^0	1.7×10^{12}	
[1] Fujii & Imura	5×10 cm	water	5.0	vertical	7.2×10^6	1.7×10^8	
[1] Fujii & Imura	30×15 cm	water	5.0	vertical	5.2×10^8	6.1×10^{10}	
[9] Hassani & Hollands	82 mm disk	air	0.71	vertical	1.4×10^0	2.7×10^5	
[9] Kobus & Wedekind	3 sizes disk	air	0.71	vertical	6.7×10^1	1.2×10^4	10%
[3] Aihara et al.	25×35 cm	air	0.71	down	7.2×10^6	1.0×10^7	
[10] Faw & Dullforce	18.1 cm disk	air	0.71	down	1.1×10^6	1.6×10^6	1.2-2.5%
[11] Goldstein & Lau	2.6-20 cm square	air	0.7	down	2.5×10^2	4.5×10^3	10%
[1] Fujii & Imura	5×10 cm	water	5.0	down	1.8×10^7	4.5×10^9	
[1] Fujii & Imura	30×15 cm	water	5.0	down	9.3×10^9	7.6×10^{11}	
[1] Fujii & Imura	5×10 cm	water	5.0	inclined	1.0×10^8		
[1] Fujii & Imura	30×15 cm	water	5.0	inclined	1.0×10^{10}		

2.3 **Measurement Data-Sets.**

There are robust measurements of natural convection heat and mass transfer in the peer-reviewed literature. Table 1 lists the data-sets to be compared with the present theory. Within each **Face** group, all Ra have been scaled to the same characteristic length metric. The "±" column is the estimated convection measurement uncertainty (scatter from Lloyd and Moran [4]) reported in the cited source. Both plates from Fujii and Imura [1] had side-walls.

Measurements were copied from the text of Aihara et al. [3], Faw and Dullforce [10], and Goldstein and Lau [11]. The remaining heat transfer measurements were captured from graphs in the cited works by measuring the distance from each point to its graph's axes, then scaling to the graph's units using the "Engauge" software. Measurements obscured by other points in the graph were excluded. [2]

[1] The conduction shape factor $q^*_{SS} = 0.932$ is used in Section 9. It is derived exactly in Section 17.

[2] Excluding the obscured points eliminates clustered points, not outliers; thus, correlations with theory will tend to be weaker than if all the points had been included.

3. Prior Work

3.1 Atmospheric Science. Rennó and Ingersoll [12] relates the "convective available potential energy" (CAPE) of a planetary atmosphere to heat-engine efficiency. Atmospheric convection is analyzed as a four phase cyclic heat-engine. They introduce "total convective available potential energy" (TCAPE) in terms of the reversible heat-engine efficiency limit $\eta = \Delta T/T$. For dry air:

$$\mathrm{TCAPE} \approx \eta\, c_p\, \Delta T \qquad \Delta T = T - T_\infty \tag{1}$$

where c_p is the fluid's specific heat (at constant pressure), T is the absolute temperature of the ground (heat-source), and T_∞ is the upper atmosphere (heat-sink) absolute temperature.

$\mathrm{CAPE} = \eta_N\, c_p\, \Delta T$, where η_N is the heat-engine efficiency of natural convection. Rennó and Ingersoll assert that $\mathrm{TCAPE} \approx 2\,\mathrm{CAPE}$. Thus, $\eta_N \approx \eta/2$.

The Goody [13] cyclic heat-engine analysis splits atmospheric convection into four phases, three of them reversible, and accounts for their energy flows and entropy.

Table 2 atmospheric convection efficiency limit

T_∞	T	η_A	η_N
240 K	300 K	10.2%	10.0%
260 K	295 K	7.7%	5.90%
250 K	295 K	7.7%	7.63%

Table 2 shows the sink (T_∞) and source (T) temperatures, the efficiency limits from Goody (η_A), and $\eta_N = \eta/2 = \Delta T/[2\,T]$. In the first row, η_A matches η_N within 2%. In the second row, η_A is 30% larger than η_N. The third row changes T_∞ from 260 K to 250 K, causing η_A and η_N to match within 1%. If "260 K" was a misprint, then both studies agree that $\eta_N \approx \eta/2$.

3.2 Upward Natural Convection From a Horizontal Plate. For upward convection heat or mass transfer from a horizontal surface, prior works [1, 2, 4, 8, 11] propose constant coefficients fitted to fractional powers of Ra, spanning various Ra ranges. The goal of this investigation being a comprehensive formula, the present theory will be compared with the measurements presented in these works, not with their piece-wise power-law approximations.

3.3 Natural Convection From a Vertical Plate. The natural convection heat transfer formula developed by Churchill and Chu [5] for a vertical rectangular isothermal plate of height L is:

$$\overline{Nu}^{1/2} = 0.825 + \frac{0.387\,Ra^{1/6}}{\left[1 + (0.492/Pr)^{9/16}\right]^{8/27}} \qquad 1 \le Ra \le 10^{12} \tag{2}$$

3.4 Downward Natural Convection From a Horizontal Plate. Schulenberg [14] derives a formula for convection below a level isothermal strip of width $2\,L$. Proposed is a corrected [3] formula and its equivalent, normalized so that Pr appears only in the denominator:

$$\overline{Nu} = \frac{0.631\,Ra^{1/5}\,Pr^{1/5}}{\left[1 + 1.56\,Pr^{3/5}\right]^{1/3}} = \frac{0.544\,Ra^{1/5}}{\left[1 + (0.477/Pr)^{3/5}\right]^{1/3}} \tag{4}$$

Schulenberg also gives a formula for downward convection from a level isothermal disk using its radius as the characteristic length. The expression on the right side is its equivalent normalized form:

$$\overline{Nu}_r = \frac{0.705\,Ra^{1/5}\,Pr^{1/5}}{\left[1 + 1.48\,Pr^{3/5}\right]^{1/3}} = \frac{0.619\,Ra^{1/5}}{\left[1 + (0.520/Pr)^{3/5}\right]^{1/3}} \tag{5}$$

[3] The Schulenberg [14] heat transfer formula for an isothermal strip was:

$$\overline{Nu} = \frac{0.571\,Ra^{1/5}\,Pr^{1/5}}{\left[1 + 1.156\,Pr^{3/5}\right]^{1/3}} = \frac{0.544\,Ra^{1/5}}{\left[1 + (0.785/Pr)^{3/5}\right]^{1/3}} \tag{3}$$

1.156 is the only 4-digit coefficient in the paper's isothermal plate correlations; the others have 3 significant digits. Figure 5 of the present work compares the effective Ra scale factor of all four of these formulas; the "1.156 Schulenberg strip $1/\Xi_?$" trace is 40% lower than the others at $Pr \ll 1$.

4. **Unenclosed Heat-Engine**

Although most textbook heat-engine analyses are of cyclic heat-engines, a continuous process can also convert a temperature difference into mechanical work, which qualifies it as a heat-engine.

Consider a large vertical column of still, dry air having molar mass M under the influence of gravitational acceleration g. Initially, the air will be in equilibrium, with uniform absolute temperature T_∞ and a pressure profile P which decays exponentially with altitude z:

$$P(z) = P_0 \exp\left(\frac{-z\, g\, M}{\overline{R}\, T_\infty}\right) \tag{6}$$

Where $\overline{R}$ is the universal gas constant, the ideal gas law finds the density ρ of a parcel of air:

$$\rho = \frac{M\, P}{\overline{R}\, T} \tag{7}$$

A heated parcel of volume V has density $\rho_h = M\, P / \left[[T_\infty + \Delta T]\, \overline{R}\right]$. The buoyancy force on it is:

$$[\rho - \rho_h]\, g\, V = \frac{g\, V\, M\, P\, \Delta T}{\overline{R}\, T_\infty\, [T_\infty + \Delta T]} \tag{8}$$

Where $0 < \Delta T \ll T_\infty$, and c_p is the specific heat (at constant pressure) of the fluid, $\Delta Q = c_p\, \rho\, V\, \Delta T$ is the heat required to raise the parcel temperature from T_∞ to $T = T_\infty + \Delta T$. The force on the parcel is:

$$[\rho - \rho_h]\, g\, V = \left[\frac{M\, P}{\rho\, \overline{R}\, T}\right] \frac{g\, \Delta Q}{c_p\, T} = \frac{g\, \Delta Q}{c_p\, T} = \frac{g\, \rho\, V\, \Delta T}{T} \tag{9}$$

As it rises, the parcel's state changes. Temperature, volume, and pressure are three variables having two degrees of freedom from Formula (7). For a large vertical column of still, dry air, Fermi [15] teaches:

> "Since air is a poor conductor of heat, very little heat is transferred to or from the expanding air, so that we may consider the expansion as taking place adiabatically."

Hence, the temperature of a parcel of dry air drops $g/c_p \approx 9.8$ K per kilometer of altitude gain. In a column having initially uniform temperature, a heated parcel will rise until its temperature drops to T_∞.

From the conservation of mass, $\rho\, V = \rho_0\, V_0$, where ρ_0 and V_0 are the density and volume at altitude $z = 0$. The maximum work W which can be extracted from a buoyant parcel is the integral of upward force Formula (9) with respect to altitude z above the heated plate:

$$W = \int_0^{\Delta T\, c_p/g} \frac{[\Delta T - z\, g/c_p]\, g\, \rho_0\, V_0}{T}\, \mathrm{d}z = \frac{g\, \Delta Q}{c_p\, T}\, \frac{\Delta T\, c_p}{2\, g} = \frac{\Delta Q\, \Delta T}{2\, T} \tag{10}$$

The thermodynamic efficiency ($W/\Delta Q$) of this ideal convection heat-engine will be the thermodynamic efficiency limit for external convection, η_N:

$$\eta_N = \frac{W}{\Delta Q} = \frac{\Delta T}{2\, T} \tag{11}$$

Note that η_N is 1/2 of the (Carnot) reversible heat-engine efficiency limit $\eta = \Delta T/T$.

This derivation was for adiabatic gases whose coefficient of thermal expansion $\beta = 1/T$. More generally:

$$\eta_N = \frac{\beta\, \Delta T}{2} \tag{12}$$

The system being in continuous operation, instead of energies W and ΔQ, power fluxes (W/m^2) are of interest. The powers per heated plate area are I_k for the kinetic flux of the fluid and I_p for the plate total, which is also the convective power flux. The thermodynamic efficiency of a steady-state convection process is I_k/I_p, which the second law of thermodynamics constrains so that:

$$\frac{I_k}{I_p} \le \eta_N \tag{13}$$

5. **Dimensional Analysis**

Additional fluid properties used in this investigation are thermal conductivity k, kinematic viscosity ν, and thermal diffusivity $\alpha = k/[\rho\, c_p]$. $\overline{h}$ is the average convective surface conductance, with units $\mathrm{W}/(\mathrm{m}^2 \cdot \mathrm{K})$.

"Scalable" heat transfer equations relate named, dimensionless "variable groups", which themselves are functions of variables and other variable groups. "Dimensional analysis" discovers these dimensionless variable groups and their scalable relationships.

Nusselt's dimensional analysis of natural convection (from Lienhard and Lienhard [7]) employs four variable groups: average Nusselt number $\overline{Nu}$, Prandtl number Pr, Π_3, and Π_4.

$$\overline{Nu} \equiv \frac{\overline{h}\, L}{k} = \frac{I_p\, L}{\Delta T\, k}, \qquad Pr \equiv \frac{\nu}{\alpha}, \qquad \Pi_3 \equiv \frac{L^3}{\nu^2}\, g = \frac{L\, g}{[\nu/L]^2}, \qquad \Pi_4 \equiv \beta\, \Delta T \tag{14}$$

The $\overline{Nu} = I_p\, L/[\Delta T\, k]$ equivalence was added for this investigation.

From these variable groups come the dimensionless Grashof number (Gr) and Rayleigh number (Ra):

$$Gr \equiv \Pi_3\, \Pi_4 = \frac{\beta\, \Delta T\, g\, L^3}{\nu^2}, \qquad Ra \equiv Gr\, Pr = \frac{\beta\, \Delta T\, g\, L^3}{\alpha\, \nu} \tag{15}$$

From Formula (12) and $\Pi_4 \equiv \beta\, \Delta T$ from Formula (14):

$$\eta_N = \frac{\Pi_4}{2} \tag{16}$$

Let Π_5 be the heat transport capacity per kinetic energy ratio. Π_5 increases with β, g, L, and Pr:

$$\Pi_5 = \beta\, g\, L\, Pr^2/c_p \tag{17}$$

The denominator c_p, canceling one of the two factors of c_p in Pr^2, makes Π_5 dimensionless.

Two variable groups with power flux units (W/m^2) will prove useful:

$$\Phi_p = \frac{k\, \Delta T}{L} \qquad \Phi_k = \left[\frac{\nu}{L}\right]^3 \rho\, \Pi_4\, \Pi_5 \tag{18}$$

6. **Combining Heat Transfers**

Conduction and convection are both heat transfer processes.

There is an unnamed form which appears frequently in heat transfer formulas:

$$F^p(\xi) = F_0^p(\xi) + F_\infty^p(\xi) \tag{19}$$

Churchill and Usagi [6] wrote that such formulas are "remarkably successful in correlating rates of transfer for processes which vary uniformly between these limiting cases."

A value of $p > 1$ models competitive processes; the combined transfer rate is between the larger constituent rate and their sum.

$p = 1$ models independent processes; the combined transfer rate is the sum of the constituent rates.

The Churchill and Chu Formula (2) for vertical plates has the form of equation (19) with $p = 1/2$. Natural convection requires some conduction to heat the fluid. This is consistent with cooperating processes having $0 < p < 1$; when both are transferring, the combination is larger than their sum.

With $F_0(\xi) \geq 0$ and $F_\infty(\xi) \geq 0$, taking the pth root of both sides of equation (19) yields a vector-space functional form known as the ℓ^p-norm, which is notated $\|F_0\ ,\ F_\infty\|_p$:

$$\|F_0\ ,\ F_\infty\|_p = (|F_0|^p + |F_\infty|^p)^{1/p} \tag{20}$$

7. Upward-Facing Circular Plate

7.1 **Characteristic Length.** For a horizontal upward-facing plate, Figure 1 shows that natural convection pulls fluid from the edges into a central plume. The characteristic length should be a function of radial distance from the edges to the center. This is accomplished by using the area-to-perimeter ratio L^* as the characteristic length L.

Lloyd and Moran [4] measured upward convection from horizontal disks, rectangles, and right triangles having aspect ratios between 1:1 and 10:1. They wrote: "It is immediately obvious that within the scatter of the data, approximately ±5 percent, the data from all plan-forms are correlated through the use of L^*, ..."

Goldstein et al. [8] found that L^* correlated their measurements with aspect ratios between 1:1 and 7:1.

7.2 **Conduction.** Consider a horizontal disk with its upper face, having area A, heated to $T_\infty + \Delta T$. Its $L = L^*$ is 1/2 of its radius. The power flowing from an object into a stationary, uniform medium is $q = S\,k\,\Delta T$, where k is thermal conductivity and S is the conduction shape factor (having length unit). For one side of a disk, Incropera, DeWitt, Bergman, and Lavine [16] gives $S = 2\,D$ $(= 8\,L^*)$. Converting conduction power flux $I_p = q/A$ into conduction Nusselt number $Nu_0^* = \overline{Nu}$ from Formula (14):

$$I_p\,A = Nu_0^*\,A\,\frac{k\,\Delta T}{L^*} = q = S\,k\,\Delta T \qquad Nu_0^* = \frac{S\,L^*}{A} = \frac{8\,L^*\,L^*}{\pi\,[2\,L^*]^2} = \frac{2}{\pi} \approx 0.637 \tag{21}$$

7.3 **Kinetic Flux.** Fluid heated near the plate converts thermal energy into kinetic energy by accelerating upward. Fluid accelerating upward spreads apart, pulling fluid horizontally to maintain its density. At some elevation z_t, the fluid no longer accelerates upward (otherwise, its velocity would be unbounded) and the horizontal flow is negligible, which is marked by the dashed line in Figure 1.

An ideal turbine at elevation z_t would capture the upward kinetic energy of the plume. The kinetic power through the aperture would be $\rho\,A\,u\,u^2/2$, where u is the plume upward velocity; its flux, $\rho\,u^3/2$.

Vertical acceleration pulls fluid horizontally at elevations between 0 and z_t. "Fig. 14(f)" of Fujii and Imura [1] shows that horizontal velocities are fairly uniform within that span. The kinetic flux should be proportional to $\rho\,u^3/2$ scaled by z_t. z_t grows with u, but shrinks with kinematic viscosity ν because of viscous losses. u/ν has reciprocal length units, while $\rho\,u^3/2$ already has power flux units. This suggests scaling $\rho\,u^3/2$ by a (dimensionless) Reynolds number $Re = u\,L/\nu$, which is used extensively for modeling forced flows. Let $Re_i = u\,L_i/\nu$, where L_i is the average length of flow parallel to the plate. For the upward-facing plate, $L_i = 2\,L = 2\,L^*$; hence $Re_i = 2\,Re$, leading to a kinetic power flux $Re\,\rho\,u^3$. From the Π_5 dimensional analysis, $Re_i\,\Pi_5\,[\rho\,u^3/2]$ is the maximum heat flux which could be transported by the flow induced by u. Multiplying this heat flux by $\Pi_4/2$ yields the maximum kinetic flux I_k which could result from natural convection:

$$I_k = Re_i\,\frac{\rho\,u^3}{2}\,\frac{\Pi_4}{2}\,\Pi_5 = \frac{\rho\,L}{2\,\nu}\,u^4\,\Pi_4\,\Pi_5 \qquad u = \left[\frac{2\,\nu\,I_k}{\rho\,L\,\Pi_4\,\Pi_5}\right]^{1/4} \tag{22}$$

7.4 **Plate Flux.** With upward convection pulling fluid horizontally from the disk's perimeter, heat transfer near the perimeter is more flow-induced than it is conduction. If the flow were parallel, 1/2 of the plate area would be considered flow-induced. If the flow were radial, 1/4 would be considered flow-induced. However, the square plate photographs in Kitamura et al. [2] show plumes as a network of connected ridge segments, not a central cone. An intermediate allocation is needed. The geometric mean of 1/2 and 1/4 is $\sqrt{1/8}$. Hence, $\sqrt{1/8} \approx 0.354$ of the plate is designated as flow-induced, $[1 - \sqrt{1/8}] \approx 0.646$ of the plate as conduction.

Heat transfer from the flow-induced part of the plate will be proportional to Nu_0^*, L^*, and Formula (22) u in the dimensionless expression $Nu_0^*\,u\,L^*/[\sqrt{8}\,\nu] = Nu_0^*\,Re/\sqrt{8}$. As cooperating processes, conductive and flow-induced heat transfers combine using the $\ell^{1/2}$-norm. Solving for plate power flux I_p from Formula (14):

$$I_p = \frac{k\,\Delta T}{L}\,Nu_0^*\left\|1 - \frac{1}{\sqrt{8}}\ ,\ \frac{Re}{\sqrt{8}}\right\|_{1/2} = \frac{k\,\Delta T}{L}\,Nu_0^*\left\|1 - \frac{1}{\sqrt{8}}\ ,\ \frac{L}{\sqrt{8}\,\nu}\left[\frac{2\,\nu\,I_k}{\rho\,L\,\Pi_4\,\Pi_5}\right]^{1/4}\right\|_{1/2} \tag{23}$$

Assume $Re \gg \sqrt{8}$, so that the $1 - \sqrt{1/8}$ term can be ignored. From definitions (18) collect Φ_k and Φ_p terms:

$$I_p = \Phi_p\,\frac{Nu_0^*}{\sqrt{8}}\left[\frac{2\,I_k}{\Phi_k}\right]^{1/4} \tag{24}$$

The I_k upper-bound can be found by combining I_p Formula (24) with η_N Formulas (13) and (16):

$$I_k \le \frac{\Pi_4}{2}\, I_p = \frac{\Phi_p\, \Pi_4\, Nu_0^*}{\sqrt{8}} \left[\frac{I_k}{8\,\Phi_k}\right]^{1/4} \tag{25}$$

Dividing both sides of Formula (25) by $I_k^{1/4}$, then raising both sides to the 4/3 power, isolates I_k:

$$I_k \le \left[\frac{\Phi_p\, \Pi_4\, Nu_0^*}{\sqrt{8}}\right]^{4/3} \left[\frac{1}{8\,\Phi_k}\right]^{1/3} = \Phi_p \left[\frac{Nu_0^*}{\sqrt{8}}\right]^{4/3} \left[\frac{\Phi_p\, \Pi_4}{\Phi_k}\right]^{1/3} \frac{\Pi_4}{2} \tag{26}$$

In the absence of obstruction, I_k and I_p will increase to the maximum allowed by upper-bound Formula (26). Substituting I_k from Formula (26) into Formula (24) yields the asymptotic formula for I_p:

$$I_p = \Phi_p \left[\frac{Nu_0^*}{\sqrt{8}}\right]^{4/3} \left[\frac{\Phi_p\, \Pi_4}{\Phi_k}\right]^{1/3} \tag{27}$$

Both I_p and I_k have $\sqrt[3]{\Phi_p\, \Pi_4/\Phi_k}$ factors. How does $\Phi_p\, \Pi_4/\Phi_k$ relate to Formula (15) Ra?

$$\frac{\Phi_p\, \Pi_4}{\Phi_k} = \frac{k\,\Delta T}{\rho\, L}\, \frac{L^3}{\nu^3}\, \frac{\beta\, g\, L}{c_p}\, \frac{\nu^2}{\alpha^2} = \frac{\beta\, \Delta T\, g\, L^3}{\alpha \nu} = Ra \tag{28}$$

$$I_p = \Phi_p \left[\frac{Nu_0^*}{\sqrt{8}}\right]^{4/3} Ra^{1/3} = \Phi_p\, \overline{Nu^*} \qquad \overline{Nu^*} = \frac{{Nu_0^*}^{4/3}}{4} Ra^{1/3} \approx 0.137\, Ra^{1/3} \tag{29}$$

Restoring the $\ell^{1/2}$-norm from equation (23) into equation (29) yields the comprehensive formula for natural convection heat transfer from an external, horizontal plate's isothermal upper face:

$$\overline{Nu^*} = \left\| Nu_0^* \left[1 - \frac{1}{\sqrt{8}}\right] \ , \ \frac{{Nu_0^*}^{4/3}}{4}\, Ra^{1/3} \right\|_{1/2} \approx \left[0.642 + 0.370\, Ra^{1/6}\right]^2 \tag{30}$$

7.5 **Measurement.** $\overline{Nu^*}$ Formula (30) assumes unobstructed flow. A completely unobstructed apparatus is difficult to build. Measurements smaller than $\overline{Nu^*}$ are expected.

Measurement bias and uncertainty can result in values slightly larger than $\overline{Nu^*}$.

8. Upward-Facing Measurements

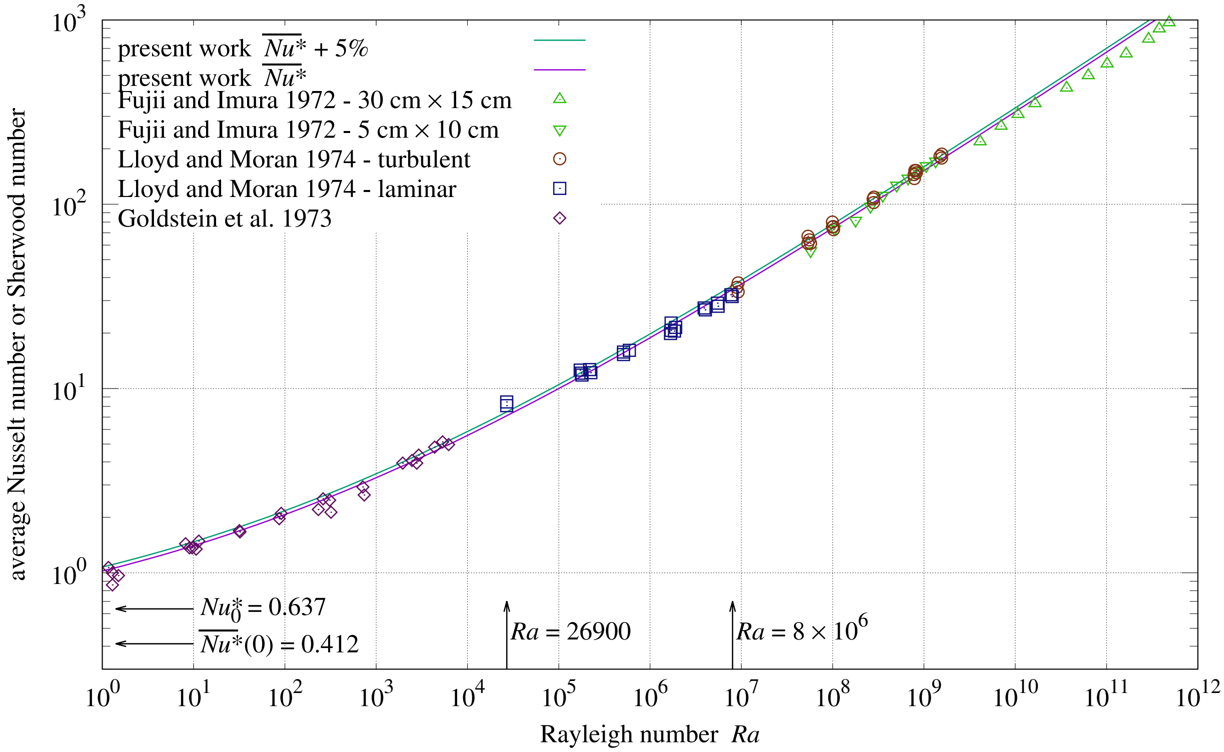

Figure 4 upward convection heat or mass transfer from horizontal plate

Table 3 upward convection mass or heat transfer from horizontal plate

Source	Data-Set	$Pr\|Sc$	Face	Formula	RMSRE	Bias	Scatter	Count
Fujii and Imura [1]	– 30 cm × 15 cm	5.0	up	(30) $\overline{Nu}^*$	12.0%	−11.4%	4.0%	11
Fujii and Imura [1]	– 5 cm × 10 cm	5.0	up	(30) $\overline{Nu}^*$	5.0%	−0.4%	5.0%	10
Lloyd and Moran [4]	– electrochemical	2200	up	(30) $\overline{Nu}^*$	4.9%	+0.7%	4.8%	39
Goldstein et al. [8]	– sublimation	2.50	up	(30) $\overline{Nu}^*$	7.2%	−2.3%	6.8%	26

Lloyd and Moran [4] estimated 5% scatter for their data. Two "Lloyd and Moran 1974 – laminar" points at $Ra \approx 26900$ have values 14% and 19% larger than $\overline{Nu}^*$ in Figure 4.

$Ra \approx 26900$ was the smallest Ra measured by Lloyd and Moran; the next smallest $Ra = 171750$ was 6.4 times larger. Range extremes are often the most susceptible to measurement bias. Having excesses several times larger than 5%, the points at $Ra \approx 26900$ should be excluded as outliers.

Excluding the two largest and two smallest measurements relative to $\overline{Nu}^*$, the Lloyd and Moran measurements have a 4.9% root-mean-squared relative error (RMSRE) from $\overline{Nu}^*$. This is a close match spanning four orders of magnitude of Ra which includes the laminar-turbulent transition at $Ra \approx 8 \times 10^6$.

8.1 **RMSRE.** RMSRE gauges the fit of measurements $g(Ra)$ to formula $f(Ra)$, giving each measurement equal weight. The root-mean-squared error of $g(Ra)$ relative to $f(Ra)$ at n points Ra_j is:

$$\sqrt{\frac{1}{n}\sum_{j=1}^{n}\left|\frac{g(Ra_j)}{f(Ra_j)}-1\right|^2} \tag{31}$$

Table 3 also splits RMSRE into bias and scatter. The root-sum-squared of bias and scatter is RMSRE.

Note that $\overline{Nu}^*(0) < Nu_0^*$ in Figure 4. $\overline{Nu}^*$ models convection; it does not extend to static conduction. The Fujii and Imura 30 cm × 15 cm upward-facing data-set is revisited in Section 21.

9. **Vertical Rectangular Plate**

9.1 Characteristic Length and Conduction. The vertical characteristic length $L' = L$ is the plate's height. Conduction constant Nu'_0 will not depend on the plate's width. The asymptotic case is a strip, an infinitely wide rectangle.

Conduction shape factors are not well-defined with unbounded source areas, but Nusselt numbers can be. Fortunately, Nu'_0 for a strip can be related to square plate Nu_0. Incropera et al. [16] gives a dimensionless shape factor $q^*_{SS} = 0.932$ for both faces of a rectangular plate. For one face of an $L \times L$ square plate:

$$A_0 = 2\,A = 2\,L^2 \qquad L_0 = \sqrt{\frac{A_0}{4\,\pi}} = \frac{L}{\sqrt{2\,\pi}} \qquad q = \frac{q^*_{SS}}{2}\,k\,\Delta T\,\frac{A}{L_0} = q^*_{SS}\,k\,\Delta T\,L\sqrt{\frac{\pi}{2}} \tag{32}$$

$$Nu_0\,A\,\frac{k\,\Delta T}{L} = q = q^*_{SS}\,k\,\Delta T\,L\sqrt{\frac{\pi}{2}} \qquad Nu_0 = q^*_{SS}\sqrt{\frac{\pi}{2}} \approx 1.168 \tag{33}$$

Strip conduction Nu'_0 must distribute over one dimension (vertical) what square plate conduction Nu_0 distributes over two:

$$Nu'_0 = {Nu_0}^2 = {q^*_{SS}}^2\,\frac{\pi}{2} \approx 1.363 \tag{34}$$

9.2 Kinetic and Plate Fluxes. Fluid is pulled horizontally before rising into a plume at the plate. The upward flow is parallel; plate area is treated as 1/2 flow-induced, 1/2 conduction. The average length of contact with the plate is $L/2$, resulting in the I_k factor $Re/2 = u\,L/[2\,\nu]$. Fluid heated by the plate accelerates upward along its surface. This reduces the effective length of contact by 1/2, resulting in $Re/4$ as the heat transfer factor in Formula (36). The kinetic and plate power fluxes are:

$$I_k = \frac{Re}{2}\,\frac{\rho\,u^3}{2}\,\frac{\Pi_4}{2}\,\Pi_5 = \frac{L}{\nu}\,\frac{\rho\,u^4}{8}\,\Pi_4\,\Pi_5 \qquad u = \left[\frac{\nu}{L}\,\frac{8\,I_k}{\rho\,\Pi_4\,\Pi_5}\right]^{1/4} \tag{35}$$

$$I_p = \frac{k\,\Delta T}{L}\,Nu'_0\left\|\frac{1}{2}\,,\;\frac{1}{2}\,\frac{Re}{4}\right\|_{1/2} = \frac{k\,\Delta T}{L}\,Nu'_0\left\|\frac{1}{2}\,,\;\frac{L}{8\,\nu}\left[\frac{\nu}{L}\,\frac{8\,I_k}{\rho\,\Pi_4\,\Pi_5}\right]^{1/4}\right\|_{1/2} \tag{36}$$

Assume $Re = u\,L/\nu \gg 1$ and ignore the conduction term; collect Φ_p and Φ_k terms from definitions (18):

$$I_p = \frac{\Phi_p}{8}\,Nu'_0\left[\frac{8\,I_k}{\Phi_k}\right]^{1/4} \tag{37}$$

The I_k upper-bound can be found by combining I_p Formula (37) with η_N Formulas (13) and (16):

$$I_k \le \frac{\Pi_4}{2}\,I_p = \frac{\Phi_p\,\Pi_4\,Nu'_0}{16}\left[\frac{8\,I_k}{\Phi_k}\right]^{1/4} \tag{38}$$

Dividing both sides of Formula (38) by $I_k^{1/4}$, then raising both sides to the 4/3 power, isolates I_k:

$$I_k \le \left[\frac{\Phi_p\,\Pi_4\,Nu'_0}{16}\right]^{4/3}\left[\frac{8}{\Phi_k}\right]^{1/3} = \Phi_p\,\frac{{Nu'_0}^{4/3}}{8\,\sqrt[3]{2}}\left[\frac{\Phi_p\,\Pi_4}{\Phi_k}\right]^{1/3}\frac{\Pi_4}{2} \tag{39}$$

The plate partially obstructs flow; $\overline{Nu'}$ will be an upper-bound. Reduce to Ra using equation (28):

$$I_p \le \frac{2}{\Pi_4}\,I_k = \Phi_p\,\frac{{Nu'_0}^{4/3}}{8\,\sqrt[3]{2}}\left[\frac{\Phi_p\,\Pi_4}{\Phi_k}\right]^{1/3} = \Phi_p\,\frac{{Nu'_0}^{4/3}}{8\,\sqrt[3]{2}}Ra^{1/3} \ge \Phi_p\,\overline{Nu'} \tag{40}$$

$$\overline{Nu'} \le \frac{{Nu'_0}^{4/3}}{8\,\sqrt[3]{2}}Ra^{1/3} \approx 0.150\,Ra^{1/3} \tag{41}$$

Reintroduce the $\ell^{1/2}$-norm into Formula (41):

$$\overline{Nu'} \le \left\|\frac{Nu'_0}{2}\,,\;\frac{{Nu'_0}^{4/3}}{8\,\sqrt[3]{2}}Ra^{1/3}\right\|_{1/2} \approx \left[0.826 + 0.387\,Ra^{1/6}\right]^2 \tag{42}$$

For large Pr, the Churchill and Chu equation (2) reduces to $\overline{Nu} = \left[0.825 + 0.387\,Ra^{1/6}\right]^2$.

The Ra term's denominator in equation (2) is always greater than 1; it can only reduce the magnitude of $\overline{Nu}$. Therefore, Formula (2) satisfies $\overline{Nu'}$ upper-bound Formula (42).

10. **Downward-Facing Rectangular Plate**

Figure 2 shows flow in two plumes on horizontally opposite sides of the plate; downward-facing characteristic length L_R is 1/2 of the shorter plate edge. Compared with the vertical convection strip, $L_R = L'/2$ and $Nu_0 = Nu'_0/2$. Plate areas are treated as 1/2 flow-induced, 1/2 conduction.

For upward-facing and vertical plates, the induced flow brings unheated fluid into contact with the plate, which is responsible for amplifying convection. In contrast, fluid below the downward-facing plate is warmed by conduction through the fluid above it. The outward creep immediately below the plate stays in contact until it reaches a plate edge. The fluid's temperature profile differs little from static conduction. Thus, static and dynamic heat transfers are combined using the ℓ^1-norm.

Figure 2 shows convective flow experiencing three 90° changes of direction. Two horizontal accelerations and decelerations of flow introduce two factors of $2\,Re = 2\,u\,L/\nu$ into I_k. The short upward acceleration and deceleration of flow below the plate is the only such occurrence among the three plate orientations. It slightly opposes buoyant flow because fluid immediately below the plate is less dense than fluid moving upward to replace it. There being no appropriate vertical distance, Re is used for the third factor in I_k.

$$I_k = 4\,Re^3\,\frac{\rho}{2}\,u^3\,\frac{\Pi_4}{2}\,\Pi_5 = \frac{L^3}{\nu^3}\,2\,\rho\,u^6\,\Pi_4\,\Pi_5 \qquad u = \left[\frac{\nu^3}{L^3}\,\frac{I_k}{2\,\rho\,\Pi_4\,\Pi_5}\right]^{1/6} \tag{43}$$

All of the lower face is in contact with horizontal flow; the heat transfer factor is $2\,Re$:

$$I_p = \frac{k\,\Delta T}{L}\,Nu_0\left[\frac{1}{2}+\frac{2\,Re}{2}\right] = \frac{k\,\Delta T}{L}\,Nu_0\left[\frac{1}{2}+\frac{L}{\nu}\left[\frac{\nu^3}{L^3}\,\frac{I_k}{2\,\rho\,\Pi_4\,\Pi_5}\right]^{1/6}\right] \tag{44}$$

Assume $u\,L/\nu \gg 1$ and ignore the conduction term; collect Φ_p and Φ_k terms; then solve for I_p:

$$I_p = \Phi_p\,Nu_0\left[\frac{I_p}{2\,\Phi_k}\right]^{1/6} \qquad I_p = \Phi_p\,\frac{{Nu_0}^{6/5}}{2^{1/5}}\,Ra^{1/5} = \Phi_p\,\overline{Nu}_R \tag{45}$$

The plate obstructs heated flow from rising; thus, $\overline{Nu}_R$ will be an upper-bound. Solving equation (45) for $\overline{Nu}_R$, restoring the ℓ^1-norm (addition), and substituting $Nu'_0/2$ for Nu_0:

$$\overline{Nu}_R \le \frac{Nu'_0}{4} + \frac{{Nu'_0}^{6/5}}{2^{7/5}}\,Ra^{1/5} \approx 0.341 + 0.550\,Ra^{1/5} \tag{46}$$

For large Pr, the Schulenberg strip convection Formula (4) reduces to $0.544\,Ra^{1/5}$. The Formula (46) coefficient 0.550 is 1.1% larger than 0.544. Being greater than 1, the denominator of Formula (4) can only reduce the magnitude of $\overline{Nu}$. Therefore, Formula (4) satisfies $\overline{Nu}_R$ upper-bound Formula (46).

11. **Generalization**

These three derivations can be generalized to equation (48) via Formulas (47). L is characteristic length; Nu_0 is static conduction; E is the count of 90° changes in direction of fluid flow; B is the sum of the mean lengths of flows parallel to the plate divided by L; C is the plate area fraction responsible for flow induced heat transfer; D is the effective length of heat transfer contact with the plate divided by L; $p = 1/2$ when $E = 1$ without side-walls; otherwise $p = 1$.

$$I_k = B\,Re^E\,\frac{\rho\,u^3}{2}\,\frac{\Pi_4}{2}\,\Pi_5 \qquad I_p = \frac{k\,\Delta T}{L}\,Nu_0\,\|1-C, C\,D\,Re\|_p \tag{47}$$

$$\overline{Nu} = \left\| Nu_0\,[1-C]\,,\ \sqrt[2+E]{[C\,D\,Nu_0]^{3+E}\,\frac{2}{B}\,Ra}\,\right\|_p \tag{48}$$

Table 4 derivation parameters

Face	**Equation**	L	Nu_0	E	B	C	D	p
up	(30) $\overline{Nu^*}$	L^*	Nu_0^*	1	2	$1/\sqrt{8}$	1	1/2
vertical	(55) $\overline{Nu'}$	L'	Nu'_0	1	1/2	1/2	1/4	1/2
down	(56) $\overline{Nu}_R$	L_R	$Nu'_0/2$	3	4	1/2	2	1

12. **Self-Obstruction of Vertical and Downward-Facing Plates**

Defined in Formula (14), the Prandtl number (Pr) is the momentum diffusivity per thermal diffusivity ratio of a fluid. Heat transfer from plates to fluids with small Pr is primarily conduction. Temperature changes in fluids with large Pr cause changes in density which induce fluid flow that transports heat. The $\overline{Nu'}$ and $\overline{Nu}_R$ upper-bound Formulas (42) and (46) are asymptotic for large Pr.

Other than as a factor of Ra, Pr does not affect upward-facing heat transfer because the heated fluid flows directly upward, as does conducted heat. When heated fluid must take longer paths around self-obstructing vertical and downward-facing plates, its heat transfer potential is reduced.

Ra scales with L^3; Pr is a property of 3-dimensional fluids. A function of Pr having values between 0 and 1 should scale Ra in the vertical and downward-facing formulas. Both Schulenberg [14] and Churchill and Chu [5] realized their formulas' dependence on Pr in this way. Expressing the denominator of vertical Formula (2) as the sixth root of an ℓ^p-norm expression named $\Xi'(Pr)$:

$$\left[1+(0.492/Pr)^{9/16}\right]^{8/27} = \left[\left\| 1\ ,\ \frac{0.492}{Pr}\right\|_{9/16}\right]^{1/6} = \left[\Xi'(Pr)\right]^{1/6} \tag{49}$$

Scaling Ra by $1/\Xi'(Pr)$ in the vertical upper-bound Formula (42) makes it equivalent to Formula (2):[4]

$$\overline{Nu}^{1/2} = 0.826 + 0.387\left[\frac{Ra}{\Xi'(Pr)}\right]^{1/6} \qquad \Xi'(Pr) = \left\| 1\ ,\ \frac{0.492}{Pr}\right\|_{9/16} \tag{50}$$

Similar treatment of the Schulenberg downward-facing strip and disk formulas (4) and (5) yields:

$$\overline{Nu} = 0.544\left[\frac{Ra}{\Xi_R(Pr)}\right]^{1/5} \qquad \Xi_R(Pr) = \left\| 1\ ,\ \frac{0.477}{Pr}\right\|_{3/5} \tag{51}$$

$$\overline{Nu} = 0.619\left[\frac{Ra}{\Xi_r(Pr)}\right]^{1/5} \qquad \Xi_r(Pr) = \left\| 1\ ,\ \frac{0.520}{Pr}\right\|_{3/5} \tag{52}$$

$$\lim_{Pr\to+0}\frac{1}{\Xi(Pr)} = 0 \qquad \lim_{Pr\to+\infty}\frac{1}{\Xi(Pr)} = 1 \tag{53}$$

The functions $\Xi'(Pr)$, $\Xi_R(Pr)$, and $\Xi_r(Pr)$ are quite similar. Coefficients 0.492, 0.477, and 0.520 are all within 5% of 1/2. This suggests using 1/2 as the coefficient in a unified function $\Xi_\forall(Pr)$. The ℓ^p-norm p parameters $3/5 = 0.6$ and $9/16 = 0.5625$ differ by less than 7%; and $\sqrt{1/3} \approx 0.577$ lies between them:

$$\Xi_\forall(Pr) = \left\| 1\ ,\ \frac{0.5}{Pr}\right\|_{\sqrt{1/3}} \tag{54}$$

Incorporating $\Xi_\forall(Pr)$ into $\overline{Nu'}$ and $\overline{Nu}_R$ upper-bound Formulas (42) and (46) creates comprehensive vertical and downward convection Formulas (55) and (56):

$$\overline{Nu'} = \left\| \frac{Nu'_0}{2}\ ,\ \frac{{Nu'_0}^{4/3}}{8\sqrt[3]{2}}\left[\frac{Ra}{\Xi_\forall(Pr)}\right]^{1/3}\right\|_{1/2} \approx \left\| 0.682\ ,\ 0.150\left[\frac{Ra}{\Xi_\forall(Pr)}\right]^{1/3}\right\|_{1/2} \tag{55}$$

$$\overline{Nu}_R = \left\| \frac{Nu'_0}{4}\ ,\ \frac{{Nu'_0}^{6/5}}{2^{7/5}}\left[\frac{Ra}{\Xi_\forall(Pr)}\right]^{1/5}\right\|_{1} \approx 0.341 + 0.550\left[\frac{Ra}{\Xi_\forall(Pr)}\right]^{1/5} \tag{56}$$

---

[4] The Ra scaling factor from Lin, Yu, and Chen [17] is $1/\Xi_L = Pr/[0.492 + 0.986\sqrt{Pr} + Pr]$; it behaves nearly identically to $1/\Xi'$.

13. *Ra* Scaling Factors

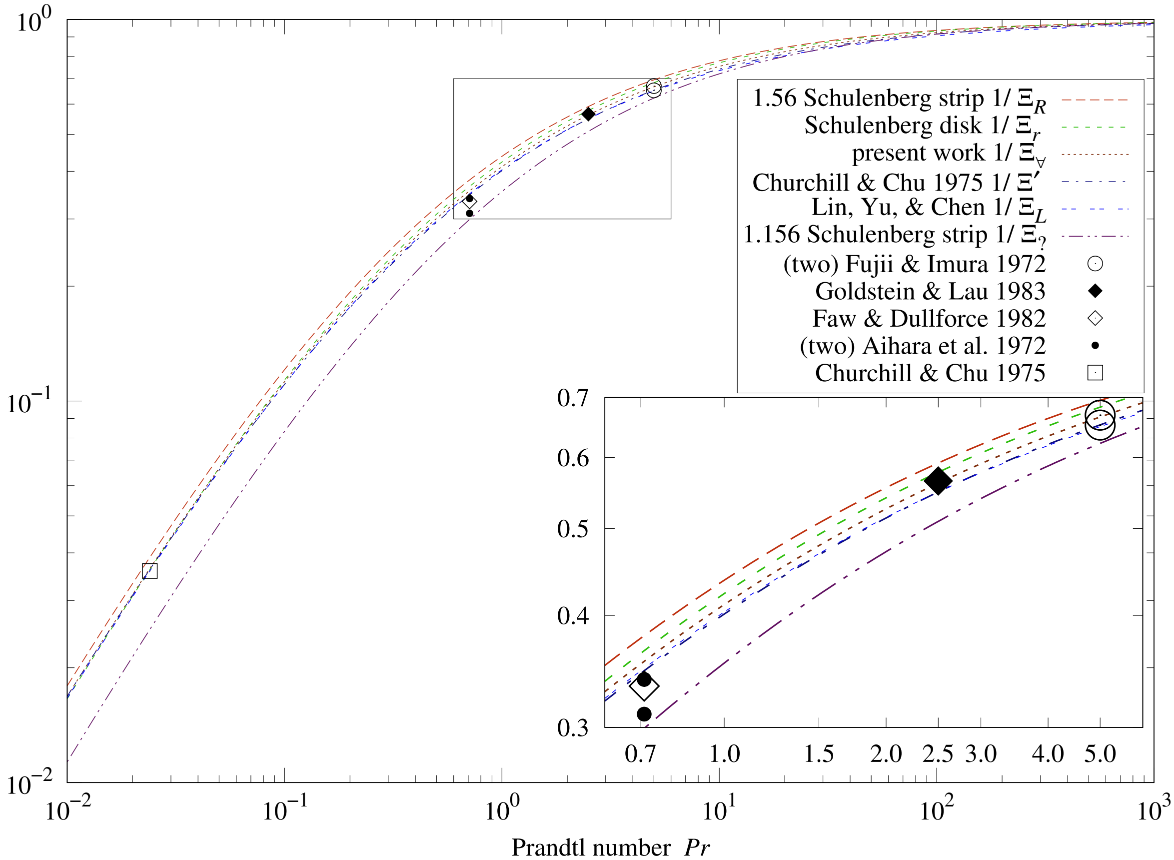

Figure 5 *Ra* **scaling functions**

Table 5 *Ra* **scaling factors**

Face	Source	Pr	Fitted	$1/\Xi_R$	$1/\Xi_r$	$1/\Xi_\forall$	$1/\Xi'$	$1/\Xi_L$	$1/\Xi_?$
vertical	Fujii & Imura [1]	5.00	0.669	-3.7%	-2.0%	+0.5%	+2.5%	+3.0%	+7.5%
down	Fujii & Imura [1]	5.00	0.652	-6.1%	-4.5%	-2.1%	-0.1%	+0.4%	+4.8%
down	Goldstein & Lau [11]	2.50	0.565	-4.5%	-2.2%	+0.6%	+2.9%	+2.9%	+10.9%
down	Faw & Dullforce [10]	0.71	0.334	-12.1%	-8.7%	-6.2%	-3.9%	-4.5%	+11.5%
down	Aihara et al. [3]	0.71	0.339	-10.7%	-7.2%	-4.7%	-2.3%	-2.9%	+13.3%
down	Aihara et al. [3]	0.71	0.310	-18.4%	-15.2%	-12.8%	-10.7%	-11.2%	+3.6%
vertical	Churchill & Chu [5]	0.024	0.036	-7.9%	-0.8%	-1.5%	-0.9%	-0.1%	+42.4%

Figure 5 presents the *Ra* scaling functions $1/\Xi(Pr)$ used in the vertical and downward-facing formulas. Also shown are $1/\Xi(Pr)$ values calculated from coefficients fitted to measurements in the cited sources.

Table 5 lists each fitted $1/\Xi$ value and its deviation from each *Ra* scaling function at the given Pr. Churchill and Chu $1/\Xi'$ is closest to the fitted values.

If a candidate formula is correct, negative deviations of fitted (aggregate) values can result from flow obstructions or measurement bias; positive deviations can result only from measurement bias.

The positive $1/\Xi'$ deviations, +2.5% and +2.9%, would indict two of the five sources in Table 5.

The positive $1/\Xi_\forall$ deviations, +0.5% and +0.6%, are tolerable.

With values between those of $1/\Xi_R$ and $1/\Xi'$, $1/\Xi_\forall$ is the most plausible of these *Ra* scaling functions.

The "1.156 Schulenberg strip $1/\Xi_?$" curve in Figure 5 is the *Ra* scaling function from Formula (3). Section 3 argues that this formula from Schulenberg [14] contained a typographical error. Being 40% less than the other curves at $Pr \ll 1$ corresponds to Formula (3) taking values 10% less than (corrected) Formula (4).

14. Vertical Measurements

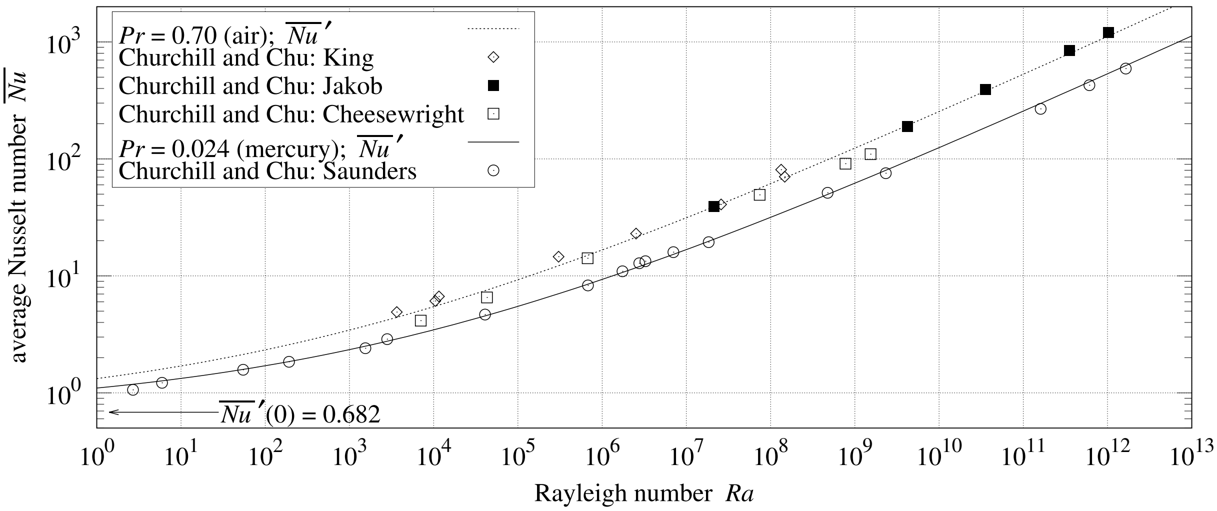

Figure 6 heat transfer from vertical rectangular plate

Table 6 heat transfer from vertical rectangular plate

Source	Data-Set	$Pr\|Sc$	Face	Formula	RMSRE	Bias	Scatter	Count
Churchill and Chu [5]	– King	0.70	vertical	(55) $\overline{Nu'}$	13.5%	+11.1%	7.6%	8
Churchill and Chu [5]	– Jakob	0.70	vertical	(55) $\overline{Nu'}$	4.7%	+3.1%	3.5%	5
Churchill and Chu [5]	– Cheesewright	0.70	vertical	(55) $\overline{Nu'}$	16.4%	−15.4%	5.6%	6
Churchill and Chu [5]	– Saunders	0.024	vertical	(55) $\overline{Nu'}$	5.3%	−1.2%	5.1%	18

Figure 6 and Table 6 present four data-sets from Churchill and Chu [5]. Differences between RMSRE computed from $\overline{Nu'}$ Formula (55) and Churchill and Chu Formula (2) are less than 1%.

15. Downward-Facing Measurements

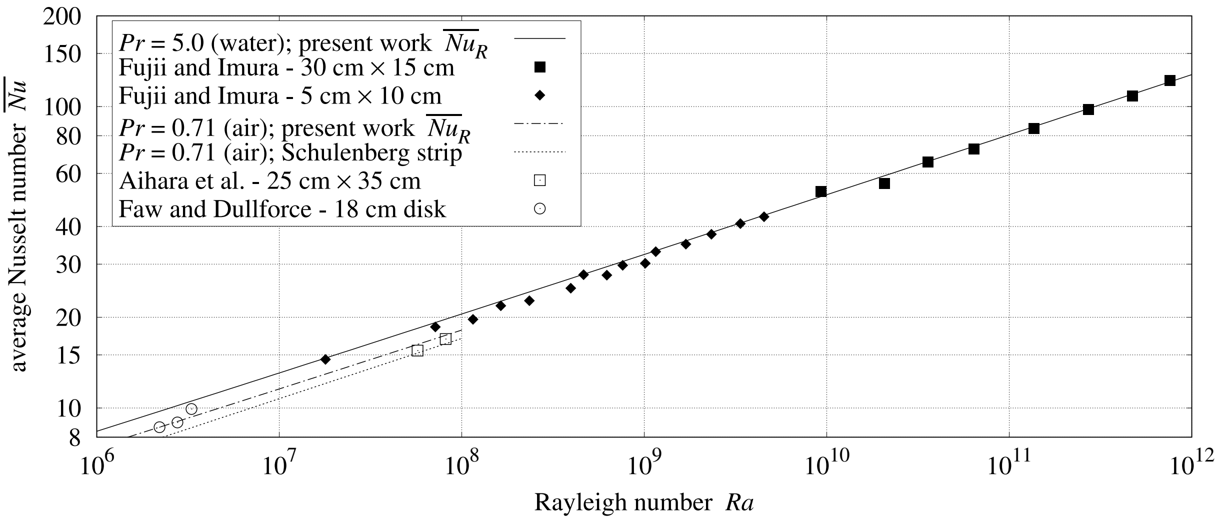

Figure 7 downward convection heat transfer from horizontal plate

Table 7 downward convection heat transfer from horizontal plate

Source	Data-Set	$Pr\|Sc$	Face	Formula	RMSRE	Bias	Scatter	Count
Fujii and Imura [1]	– 30 cm × 15 cm	5.0	down	(56) $\overline{Nu}_R$	2.7%	−0.8%	2.6%	8
Fujii and Imura [1]	– 5 cm × 10 cm	5.0	down	(56) $\overline{Nu}_R$	4.2%	−3.4%	2.5%	15
Aihara et al. [3]	– 25 cm × 35 cm	0.71	down	(56) $\overline{Nu}_R$	3.8%	−3.7%	0.9%	2
Faw and Dullforce [10]	– 18.1 cm disk	0.71	down	(56) $\overline{Nu}_R$	3.7%	+1.8%	3.2%	3

16. Characteristic Length Metrics

For upward convection, L^* (area-to-perimeter ratio) is well-defined for any flat, convex plate.

The formulas for vertical (55) and downward convection (56) were developed for rectangular plates. More general characteristic length metrics are needed to model heat transfer from other plate shapes.

The next sections develop new characteristic length metrics for vertical and downward-facing plates, and re-derive the formulas for $\overline{Nu^*}$ (30), $\overline{Nu'}$ (55), and $\overline{Nu}_R$ (56) from alternative plate shapes.

17. Downward-Facing Circular Plate

Schulenberg equations (4) and (5) for downward-facing strips and disks have matching exponents, but their coefficients and characteristic lengths differ: L_R is 1/2 of the rectangle's shorter side, versus disk radius R. Can $\overline{Nu}_R$ Formula (56) predict heat transfer for both shapes using a single characteristic length metric?

17.1 **Harmonic Mean.** Figure 2 shows fluid closest to the heated surface flowing outward from the mid-line. If the plate edge is at varying distances from the mid-line (in the direction of flow), then some sort of length averaging is needed. Flow will be faster over the shorter distances because it experiences less drag; this suggests use of the "harmonic mean", in which small values have more influence than large.

For rectangles and disks, the mid-line is one of the plate's equal-area bisectors. For rectangles it is parallel to the longer sides; but it is not the longest bisector, which is a diagonal. Being parallel to the longer sides implies that the mid-line is perpendicular to the shorter sides. It will also be perpendicular to the shortest equal-area bisector; and this works for disks as well, where all diameters are bisectors.

Consider a flat heated surface with its convex perimeter defined by functions $y_+(x) > 0$ and $y_-(x) < 0$ within the range $-R < x < R$ along the equal-area bisector which is perpendicular to the shortest equal-area bisector. Let L_R be the combined harmonic mean of $|y_+(x)|$ and $|y_-(x)|$:

$$L_R = 1 \Bigg/ \int_{-R}^{R} \left[\frac{1}{|y_+(x)|} + \frac{1}{|y_-(x)|}\right] \frac{\mathrm{d}x}{4\,R} \tag{57}$$

For rectangular plates, L_R Formula (57) is 1/2 of the shorter side's length, the same characteristic length used by Schulenberg [14]. For disks of radius R:

$$y_+(x) = -y_-(x) = \sqrt{R^2 - x^2} \qquad L_R = 4\,R \Bigg/ \int_{-R}^{R} \frac{2}{\sqrt{R^2 - x^2}}\,\mathrm{d}x = \frac{2}{\pi}\,R \tag{58}$$

Schulenberg's disk Formula (5) used radius R as the disk's characteristic length. Converting the $\overline{Nu}_r$ coefficient from characteristic length R to L_R is $0.619\,[2/\pi]^{1/5} \approx 0.566$, which is within 3% of the 0.550 coefficient of $\overline{Nu}_R$ formula (56).

17.2 **Recalculate Conduction.** The derivation of downward Formulas (46, 56) was for a square plate. To derive the downward formula for a disk, Nu_0 will be recalculated; it will be scaled larger because of the increased flow over the shorter distances. Recalling from Section 7, the conduction shape factor for one side of a disk is $S = 2\,D = 4\,R$.

$$Nu_0 = \frac{S\,L_R}{A} = \frac{4\,R\,L_R}{\pi\,R^2} = \frac{8}{\pi^2} \approx 0.811 \tag{59}$$

Upward-facing disk Nu_0^* was scaled by $\sqrt{1/8}$ in Formula (27) because its flow was midway between parallel and radially inward; downward-facing $Nu_0'/2$ was unscaled in (rectangle) Formula (44). The flow from a downward-facing disk spreads from a diameter; an intermediate scale is needed. The geometric mean of 1 (unscaled) and $\sqrt{1/8}$ is $\sqrt[4]{1/8}$. Scaling Nu_0 by the reciprocal, $\sqrt[4]{8} \approx 1.682$, yields the rectangular $Nu_0' \approx 1.363$. With the L_R harmonic mean metric (57) and $\sqrt[4]{8}\,Nu_0 = Nu_0'$, the rest of the derivation is unchanged. Thus, downward Formula (56) works for both rectangular and circular plates.

17.3 **Measurements.** Figure 7 and Table 7 include three disk measurements from Faw and Dullforce [10].

17.4 **Rectangle Shape Factor.** $\sqrt[4]{8}\,Nu_0 = Nu_0'$ derives an exact expression for the rectangular plate's dimensionless shape factor q_{SS}^*:

$${q_{SS}^*}^2\,\frac{\pi}{2} = \frac{8\,\sqrt[4]{8}}{\pi^2} \qquad q_{SS}^* = \frac{4\,\sqrt[8]{8}}{\pi^{3/2}} \approx 0.93158+ \tag{60}$$

18. **Vertical Circular Plate**

Consider a flat vertical plate as an array of narrow vertical plates. With $Ra = 0$, integrate h across the vertical slices of heights $L(x)$; then solve $\overline{h} = Nu'_0\,k/L'$ for L':

$$\frac{Nu'_0\,k}{L'} = \overline{h} = \frac{1}{2\,R}\int_{-R}^{R}\frac{Nu'_0\,k}{L(x)}\,\mathrm{d}x \qquad L' = 2\,R \Bigg/ \int_{-R}^{R}\frac{1}{L(x)}\,\mathrm{d}x \tag{61}$$

Therefore, the vertical characteristic length L' is the harmonic mean of vertical spans $L(x)$.

For a rectangle of height L, $L' = L$. For the disk of radius R, $L' = 4\,R/\pi$. Recalculating Nu_0:

$$Nu_0 = \frac{S\,L'}{A} = \frac{4\,R\,L'}{\pi\,R^2} = \frac{16}{\pi^2} \approx 1.621 \tag{62}$$

Instead of the bifurcated flow from the downward-facing plate, flow is along full vertical spans of the disk; 1/2 of the diameter-to-circle fringing which scaled downward-facing disk Nu_0 by $\sqrt[4]{8}$ should apply to vertical disks. With this scaling, $Nu_0\,\sqrt[4]{8}/2 = Nu_0/\sqrt[4]{2} = Nu'_0 \approx 1.363$, and the rest of the derivation is unchanged. Thus, vertical Formula (55) works for disks and axis-aligned rectangular plates using L' harmonic mean Formula (61).

18.1 **Measurements.** Kobus and Wedekind [9] measured natural convection heat transfer from vertical thermistor disks in air. They also included a series of similar measurements from Hassani and Hollands (1987). Pr was not specified; 0.71 is assumed. Each disk's diameter d and thickness t are specified in Figure 8.

Air heated by the two disk sides flows over the upper half of the rim, inhibiting upper rim heat transfer. The lower half of the rim transfers heat at the same per area rate as the sides. The disk effective surface area, including half of the rim, is $\pi\,d^2/2 + \pi\,d\,t/2$. Being normalized for area, $\overline{Nu'}$ should be scaled by:

$$\frac{\pi\,d^2/2}{\pi\,d^2/2 + \pi\,d\,t/2} = \frac{d^2}{d^2 + d^2\,[t/d]} = \frac{1}{1 + t/d} \tag{63}$$

To convert characteristic lengths to the harmonic mean, Kobus and Wedekind Ra gets scaled by $[2/\pi]^3$; $\overline{Nu}$ gets scaled by $[2/\pi]$ and Formula (63). Hassani and Hollands used different characteristic lengths for Ra and $\overline{Nu}$; their Ra gets scaled by $1/[2\,\sqrt{\pi}]^3$, while $\overline{Nu}$ gets scaled by $\sqrt{\pi}/4$ and Formula (63).

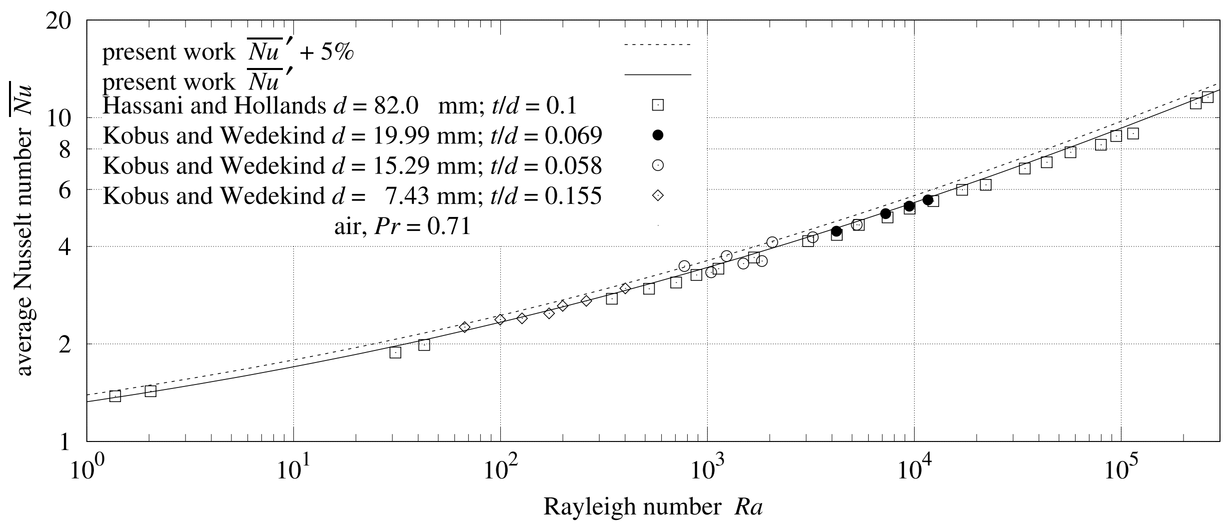

Figure 8 heat transfer from vertical disk

Table 8 heat transfer from vertical disk

Source	Data-Set	$Pr\|Sc$	Face	Formula	RMSRE	Bias	Scatter	Count
Hassani and Hollands [9]	– 82 mm	0.71	vertical disk	(55) $\overline{Nu'}$	3.8%	−3.4%	1.6%	26
Kobus and Wedekind [9]	– three sizes	0.71	vertical disk	(55) $\overline{Nu'}$	3.2%	−0.4%	3.1%	19

Figure 8 and Table 8 present the vertical disk heat transfer measurements.

In the clever design using thermistors, only horizontal clearance and the wires attached to the disk centers remained as obstructions, achieving a close match with the present theory in Table 8.

19. **Upward-Facing Square Plate**

Converting square plate Nu_0 Formula (33) from L' to L^* is division by 4. Expanding q^*_{SS} from equation (60):

$$\frac{Nu_0}{4} = \frac{q^*_{SS}}{4}\sqrt{\frac{\pi}{2}} = \frac{\sqrt[8]{8}}{\sqrt{2}\,\pi} = \frac{8^{5/8}}{4\,\pi} \approx 0.292 \tag{64}$$

The square plate's flow will be moderately radial, scaling midway between the reciprocal of $\sqrt{1/8}$ from the upward-facing disk, and $\sqrt[4]{8}$ from the downward-facing disk's bifurcated flow. The geometric mean of $\sqrt{8}$ and $\sqrt[4]{8}$ is $8^{3/8} \approx 2.181$. Scaling $Nu_0/4$ by $8^{3/8}$ yields $2/\pi = Nu^*_0 \approx 0.637$ from equation (21). The rest of the derivation is unchanged. Thus, upward convection $\overline{Nu^*}$ Formula (30) works for disks and square plates.

20. **Vertical Rectangular Plate With Side-Walls**

The Fujii and Imura [1] apparatus had (unheated) perpendicular side-walls of length L' forming a channel with the plate. In Table 9, the vertical 30 cm and 5 cm plates average 44% and 18% less heat transfer than expected by $\overline{Nu'}$ vertical Formula (55). Clearly, Formula (55) is incorrect for vertical plates with side-walls.

Formula (65) incorporates an additional factor of Re in I_k to model the side-wall drag. The side-walls obstruct horizontal flow, so the combined length of flow along the plate and side-wall is $2\,L$; heat transfer contact along the plate is L. The $\ell^{1/2}$-norm changes to the ℓ^1-norm

$$I_k = 2\,Re\,Re\,\frac{\rho\,u^3}{2}\,\frac{\Pi_4}{2}\,\Pi_5 = \frac{L^2}{\nu^2}\,\frac{\rho\,u^5}{2\,\Pi_4\,\Pi_5} \qquad u = \left[\frac{\nu^2}{L^2}\,\frac{2\,I_k}{\rho\,\Pi_4\,\Pi_5}\right]^{1/5} \tag{65}$$

$$I_p = \frac{k\,\Delta T}{L}\,Nu'_0\,\left\|\frac{1}{2}\,,\,\frac{1}{2}\,Re\right\|_1 = \frac{k\,\Delta T}{L}\,Nu'_0\,\left[\frac{1}{2} + \frac{L}{2\,\nu}\,\left[\frac{\nu^2}{L^2}\,\frac{2\,I_k}{\rho\,\Pi_4\,\Pi_5}\right]^{1/5}\right] \tag{66}$$

Using the general Formula (48) with $E = 2$, $B = 2$, and $D = 1$:

$$\overline{Nu'}_w = \frac{Nu'_0}{2} + \frac{{Nu'_0}^{5/4}}{2^{5/4}}\,\left[\frac{Ra}{\Xi_\forall(Pr)}\right]^{1/4} \tag{67}$$

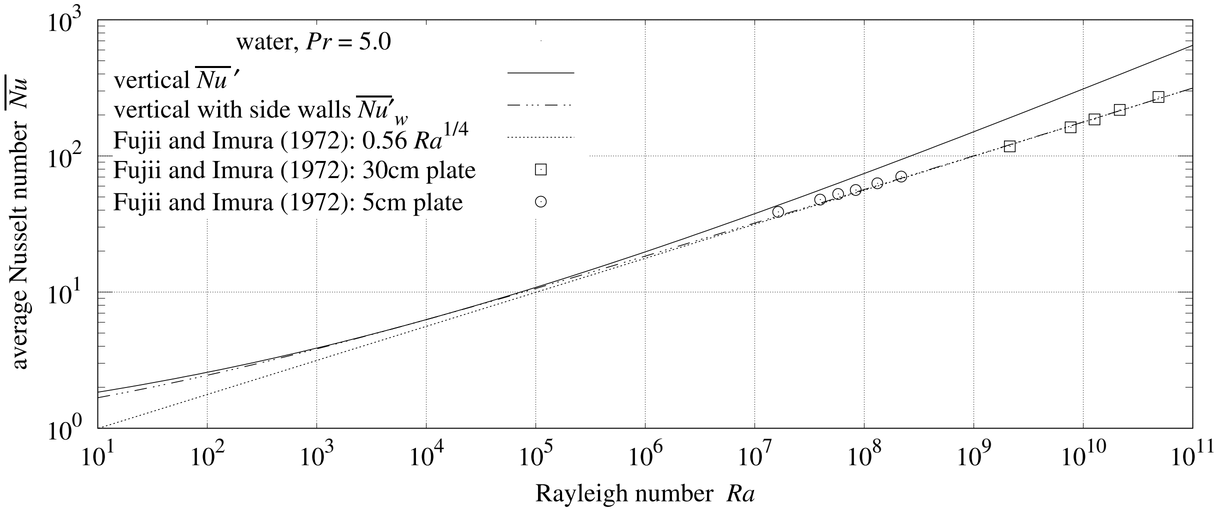

Figure 9 vertical Fujii and Imura plates

Table 9 vertical Fujii and Imura plates

Source	Data-Set	$Pr\|Sc$	Face	Formula	RMSRE	Bias	Scatter	Count
Fujii and Imura [1] –	30 cm × 15 cm	5.0	vertical	(55) $\overline{Nu'}$	43.8%	−43.7%	3.0%	5
Fujii and Imura [1] –	30 cm × 15 cm	5.0	vertical	(67) $\overline{Nu'}_w$	2.2%	−0.5%	2.2%	5
Fujii and Imura [1] –	5 cm × 10 cm	5.0	vertical	(55) $\overline{Nu'}$	18.9%	−18.3%	4.7%	6
Fujii and Imura [1] –	5 cm × 10 cm	5.0	vertical	(67) $\overline{Nu'}_w$	5.2%	+5.0%	1.6%	6

Table 9 details the performance of Formula (67) for vertical plates with side-walls. RMSRE of 2.2% and 5.2% are substantial decreases from 43.8% and 18.9%. Figure 9 shows $\overline{Nu'}_w \le \overline{Nu'}$, as required by efficiency constraints.

21. Upward-Facing Rectangular Plate With Side-Walls

The L^*_w area-to-perimeter ratio for side-walled upward-facing plates excludes side-wall length L' from the perimeter length $(2\,w + 2\,L')$ because there is no flow through side-walls. Thus, $L^*_w = L'\,w/[2\,w] = L'/2$.

In Table 3 (and Table 10), the Fujii and Imura data-sets averaged 0.4% and 11.4% less than expected from $\overline{Nu}^*$ Formula (30). The 30 cm plate having side-walls twice as long as its 15 cm channel width made its flow similar to vertical plate flow in each half of the plate towards the center-line. $L = L^*_w = L'/2$.

Fluid rises after heating; so the I_k and heat transfer factors are both $Re/2$. As with the side-walled vertical plate, conduction and flow-induced heat transfer combine using the ℓ^1-norm (addition):

$$I_k = \frac{Re}{2}\,\frac{\rho\,u^3}{2}\,\frac{\Pi_4}{2}\,\Pi_5 = \frac{L}{\nu}\,\frac{\rho\,u^4}{8\,\Pi_4\,\Pi_5} \qquad u = \left[\frac{\nu}{L}\,\frac{8\,I_k}{\rho\,\Pi_4\,\Pi_5}\right]^{1/4} \tag{68}$$

$$I_p = \frac{k\,\Delta T}{L}\,\frac{Nu'_0}{2}\,\left\|\frac{1}{2}\,,\;\frac{1}{2}\,\frac{Re}{2}\right\|_1 = \frac{k\,\Delta T}{L}\,Nu'_0\,\left\|\frac{1}{4}\,,\;\frac{L}{8\,\nu}\,\left[\frac{\nu}{L}\,\frac{8\,I_k}{\rho\,\Pi_4\,\Pi_5}\right]^{1/4}\right\|_1 \tag{69}$$

Flow is partially obstructed by the side walls; hence, Ra will be scaled by $1/\Xi(Pr)$. Using the general Formula (48) with $Nu_0 = Nu'_0/2$, $B = 1/2$, $C = 1/2$, $D = 1/2$, and $p = 1$:

$$\overline{Nu}_w = \frac{Nu'_0}{4} + \frac{{Nu'_0}^{4/3}}{8\,\sqrt[3]{2}}\,\left[\frac{Ra'}{\Xi(Pr)}\right]^{1/3} \tag{70}$$

Note that, unlike $\overline{Nu}^*$ Formula (30), $\overline{Nu}_w$ Formula (70) depends on $\Xi(Pr)$.

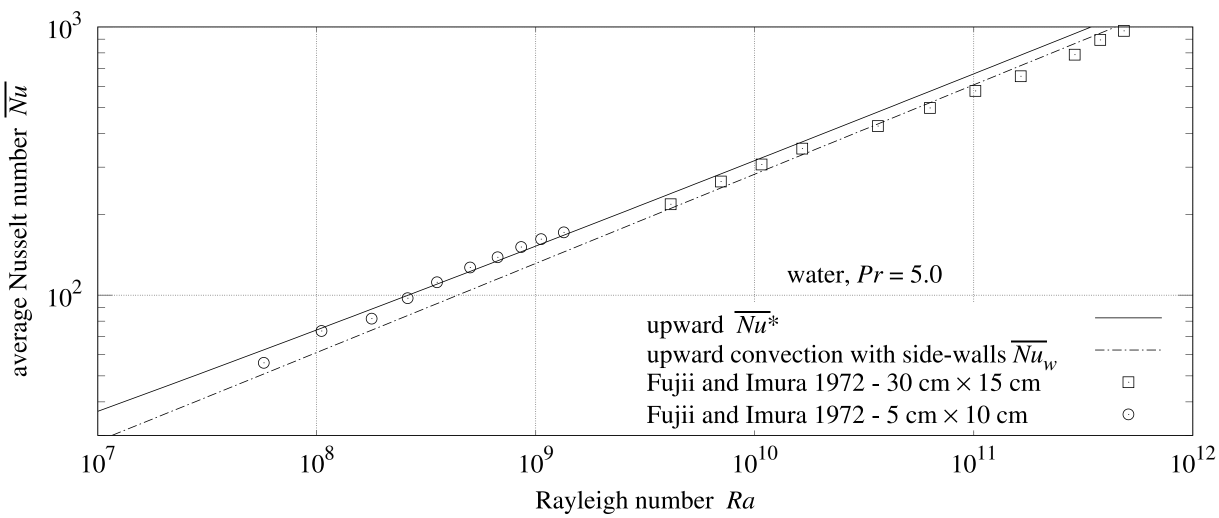

Figure 10 upward-facing Fujii and Imura plates

Table 10 upward-facing Fujii and Imura plates

Source	Data-Set	$Pr\|Sc$	Face	Formula	RMSRE	Bias	Scatter	Count
Fujii and Imura [1]	– 30 cm × 15 cm	5.0	up	(30) $\overline{Nu}^*$	12.0%	−11.4%	4.0%	11
Fujii and Imura [1]	– 30 cm × 15 cm	5.0	up	(70) $\overline{Nu}_w$	6.0%	−1.8%	5.7%	11
Fujii and Imura [1]	– 5 cm × 10 cm	5.0	up	(30) $\overline{Nu}^*$	5.0%	−0.4%	5.0%	10
Fujii and Imura [1]	– 5 cm × 10 cm	5.0	up	(70) $\overline{Nu}_w$	18.2%	+17.7%	4.1%	10

Figure 10 and Table 10 show that $\overline{Nu}_w$ Formula (70) is effective for the 30 cm plate, but not for the 5 cm plate. The 5 cm plate's 10 cm channel width is twice the 5 cm side-wall length. This makes its flow more radial than parallel. Thus, $\overline{Nu}^*$ Formula (30) is more appropriate for the 5 cm plate. Table 11 lists the general derivation formula(48) parameters for the side-wall flow topologies.

Table 11 side-walled plate parameters

Face	Equation	L	Nu_0	E	B	C	D	p
up	(70) $\overline{Nu}_w$	$L^*_w = L'/2$	$Nu'_0/2$	1	1/2	1/2	1/2	1
vertical	(67) $\overline{Nu'}_w$	L'	Nu'_0	2	2	1/2	1	1

22. Inclined Plate

Let θ be the angle of a plate from vertical. Face up $\theta = -90°$; vertical $\theta = 0°$; face down $\theta = +90°$. This investigation has derived and tested formulas for rectangular and circular plates at $-90°$, $0°$, and $+90°$.

Following Fujii and Imura [1], the Ra' argument to vertical Formula (55) gets scaled by $|\cos\theta|$ to model the reduced vertical convection from an inclined plate. [5] Following Raithby and Hollands [18], the Ra^* and Ra_R arguments to the upward and downward formulas (30) and (56) get scaled by $|\sin\theta|$.

Raithby and Hollands take the maximum convective surface conductance $\overline{h} = k\,\overline{Nu}/L$, not $\overline{Nu}$, to determine the overall convection. This is because $\overline{Nu'}$, $\overline{Nu^*}$, and $\overline{Nu_R}$ have different characteristic lengths, while $\overline{h}$ is independent of L. Taking the maximum asserts that the associated flow topologies are mutually exclusive. This extreme competition is the ℓ^∞-norm, which is equivalent to the max( ) function when all its arguments are non-negative:

$$\overline{h} = k \begin{cases} \max\left(\overline{Nu'}(|\cos\theta|\,Ra')/L', \overline{Nu}_R\left(|\sin\theta|\,Ra_R\right)/L'\right) & \Delta T\,\sin\theta \ge 0 \\ \max\left(\overline{Nu'}(|\cos\theta|\,Ra')/L', \overline{Nu^*}(|\sin\theta|\,Ra^*)/L^*\right) & \Delta T\,\sin\theta \le 0 \end{cases} \tag{71}$$

Rayleigh numbers can be expressed in terms of (vertical plate) Ra':

$$\overline{h} = k\,\max\left(\frac{\overline{Nu'}(|\cos\theta|\,Ra')}{L'}, \frac{1}{L_R}\,\overline{Nu}_R\left(|\sin\theta|\,Ra'\left[\frac{L_R}{L'}\right]^3\right)\right) \qquad \Delta T\,\sin\theta \ge 0 \tag{72}$$

$$\overline{h} = k\,\max\left(\frac{\overline{Nu'}(|\cos\theta|\,Ra')}{L'}, \frac{1}{L^*}\,\overline{Nu^*}\left(|\sin\theta|\,Ra'\left[\frac{L^*}{L'}\right]^3\right)\right) \qquad \Delta T\,\sin\theta \le 0 \tag{73}$$

The downward-facing topology flows outward from opposite plate edges; there is no plate area available for the vertical flow topology. Thus, $\overline{Nu'}$ and $\overline{Nu}_R$ are mutually exclusive in Formula (72). The upward-facing topology draws fluid from the whole perimeter. Thus, $\overline{Nu'}$ and $\overline{Nu^*}$ are mutually exclusive in Formula (73). Note that Formula (73) mutual exclusion may not hold when part of the perimeter flow is obstructed.

Ideally, when $Ra = 0$, $\overline{h}$ should be independent of θ. For a 1 m square plate in $k = 1$ fluid, $\overline{h}(0°) = \overline{h}(+90°) = {Nu_0}'/2 \approx 0.682$, but $\overline{h}(-90°) \approx 1.646$. When $\theta = -90°$ forces $Ra'\,\cos\theta$ to 0, only the conduction term remains. As noted in Section 8, $\overline{Nu^*}$ Formula (30) does not extend to static conduction.

$\overline{Nu^*}$ and $\overline{Nu'}$ track measurements well near $Ra \approx 1$ in Figures 4, 6, and 8. Ignoring $\overline{Nu^*}$ when $Ra'\sin\theta > -[L^*/L']^3$, and $\overline{Nu}_R$ when $Ra'\sin\theta < [L_R/L']^3$, avoids the conduction term competition at $\theta \approx 0$:

$$\overline{h} = k \begin{cases} \max\left(\overline{Nu'}(|\cos\theta|\,Ra')/L', \overline{Nu^*}\left(|\sin\theta|\,Ra'\,[L^*/L']^3\right)/L^*\right) & Ra'\sin\theta < -[L^*/L']^3 \\ \max\left(\overline{Nu'}(|\cos\theta|\,Ra')/L', \overline{Nu}_R\left(|\sin\theta|\,Ra'\,[L_R/L']^3\right)/L_R\right) & Ra'\sin\theta > [L_R/L']^3 \\ \overline{Nu'}\left(|\cos\theta|\,Ra'\right)/L' & \text{otherwise.} \end{cases} \tag{74}$$

Note that $L^*/L' \le 1/2$ and $L_R/L' \le 1/2$ are true for any flat, convex plate face.

For $Ra > 1$, the proposed $\overline{h}$ Formula (74) will match non-side-walled horizontal and vertical plate measurements to their appropriate $k\,\overline{Nu^*}/L^*$, $k\,\overline{Nu'}/L'$, and $k\,\overline{Nu}_R/L_R$ values.

23. Inclined Plate With Side-Walls

The Fujii and Imura [1] apparatus had length L' side-walls. In Table 7, $\overline{Nu}_R$ Formula (56) has less than 5% RMSRE; it is used as the side-walled downward-facing formula with $L_R = L'/2$, regardless of which side is shorter.

To adapt $\overline{h}$ formulas (72) and (73) to apparatus with side-walls, $\overline{Nu'}_w$ Formula (67) replaces $\overline{Nu'}$. This leads to proposed downward $\overline{h}$ Formula (75) for side-walled plates:

$$\overline{h} = k\,\max\left(\frac{\overline{Nu'}_w(|\cos\theta|\,Ra')}{L'}, \frac{\overline{Nu}_R\left(|\sin\theta|\,Ra'/2^3\right)}{L'/2}\right) \qquad \Delta T\,\sin\theta \ge 0 \tag{75}$$

Fujii and Imura photographs show the plume originating in the middle of the 5 cm plate when $\theta = -90°$. The origin shifts 9% toward the elevated end of the plate when $\theta = -85°$. The plume for the 30 cm plate at $\theta = -60°$ originates in the upper 1/4 of the plate. Plume movement with θ indicates that regions of upward-facing and vertical convection shared the side-walled plate in the Fujii and Imura apparatus.

[5] Fujii and Imura [1] credits B. R. Rich with the idea of scaling vertical Ra by $|\cos\theta|$. It can be thought of as a reduction in the effective gravitational acceleration g, which scales Ra linearly.

The side-walled upward and vertical topologies compete for horizontal flow in the channel. If competition were between perpendicular flows, they would combine as the root-sum-squared, which is the ℓ^2-norm. To compete for horizontal channel flow, two changes in direction are required; they combine as the ℓ^4-norm.

The 30 cm plate has side-walls twice as long as its channel width w. Flow through this channel will be primarily parallel, as modeled by $\overline{Nu}_w$ Formula (70). The proposed upward $\overline{h}$ formula for the 30 cm plate is:

$$\overline{h} = k \left\| \frac{\overline{Nu'}_w(|\cos\theta|\,Ra')}{L'} \;,\; \frac{\overline{Nu}_w\left(|\sin\theta|\,Ra'/2^3\right)}{L'/2} \right\|_4 \qquad \Delta T\,\sin\theta \le 0 \qquad w < L' \tag{76}$$

The 5 cm plate's 10 cm channel is twice as wide as its length; horizontal flow will be more radial than parallel. At $\theta = -90°$ it is modeled by $\overline{Nu^*}$ Formula (30), but with characteristic length $L^*_w = L'/2$.

Fujii and Imura streamlines photographs show the vertical $\overline{Nu'}_w$ and upward-facing $\overline{Nu}_w$ flow modes having uniform rates of horizontal flow between the lower heated plate edge and pause elevation z_t.

Uniform horizontal flow is not the case for the 5 cm plate at $\theta = -45°$. The horizontal flow is slower near the lower plate edge and increases with elevation. The plume lacks a clear origin. It does not match any flow topology described thus far.

The upward-facing flow topology has bilateral symmetry; there is no flow between the halves created by severing along a plane of symmetry. Thus, half of the upward-facing flow topology is also a flow topology. Its general Formula (48) parameters are the same as the upward-facing topology, except that $L = 2\,L^*$. The $\theta = -45°$ flow topology is modeled as the ℓ^4-norm of $\overline{h'}_w$ and $\overline{h^*}/2$, where $\overline{h^*}/2$ is the heat transfer from this half upward flow topology. The proposed upward $\overline{h}$ formula for the 5 cm plate is:

$$\overline{h} = k \left\| \frac{\overline{Nu'}_w(|\cos\theta|\,Ra')}{L'} \;,\; \frac{\overline{Nu^*}\left(|\sin\theta|\,Ra'/2^3\right)}{L'/\gamma(\theta)} \right\|_4 \qquad \Delta T\,\sin\theta \le 0 \tag{77}$$

$$\gamma(\theta) = \max\left(1, \min\left(2, |\tan\theta| + 1 - w/L'\right)\right) \qquad w > L' \tag{78}$$

At $\theta = -90°$, heat transfer is $\overline{h^*}$; so $\gamma(-90°) = 2$. At $\theta = -45°$, it is $\left\|\overline{h'}_w \,,\, \overline{h^*}/2\right\|_4$; so $\gamma(-45°) = 1$. The transition between $\gamma = 2$ and $\gamma = 1$ depends on θ, w, and L'. Dimensional analysis yielding Formula (78) localizes the transition to $w/L < |\tan\theta| < w/L + 1$, whose bounds are marked by arrows in Figure 11.

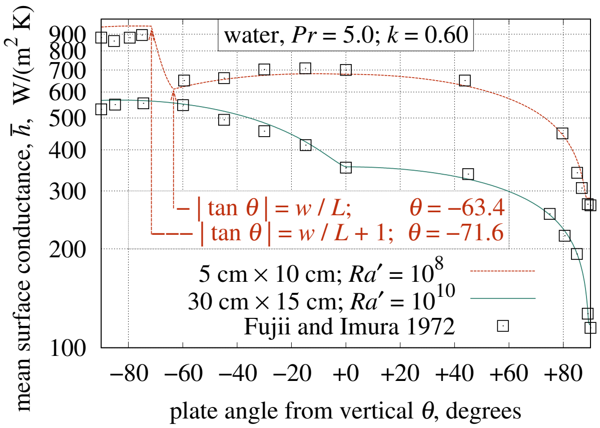

Figure 11 inclined Fujii and Imura plates

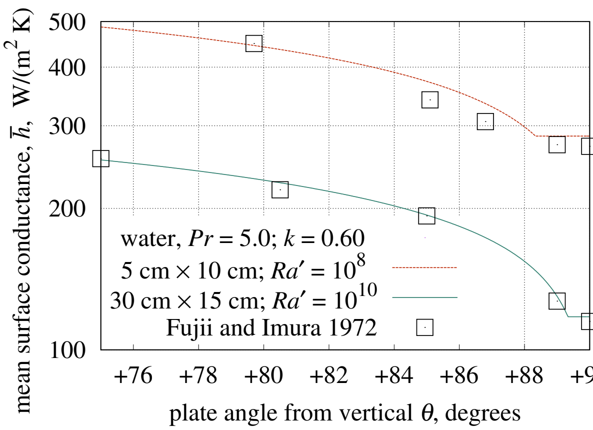

Figure 12 inclined plate detail

Table 12 inclined plate heat transfer

Source	Data-Set	$Pr\|Sc$	Face	Formula	RMSRE	Bias	Scatter	Count
Fujii and Imura [1] – 5 cm × 10 cm		5.0	inclined	(75, 77) $\overline{h}$	5.8%	−2.4%	5.3%	15
Fujii and Imura [1] – 30 cm × 15 cm		5.0	inclined	(75, 76) $\overline{h}$	3.3%	−2.2%	2.6%	14

Tables 7, 9, 10, and 12 show that the present theory is sufficient to explain, with RMSRE between 2.2% and 6.0%, the Fujii and Imura heat transfer measurements of horizontal, vertical, and inclined plates.

24. Results

Table 13 measurements versus present theory

Source	Data-Set	$Pr\|Sc$	Face	Formula	RMSRE	Bias	Scatter	Count
Goldstein et al. [8] – sublimation		2.50	up	(30) $\overline{Nu^*}$	7.2%	−2.3%	6.8%	26
Fujii and Imura [1] – 30 cm × 15 cm		5.0	up	(70) $\overline{Nu}_w$	6.0%	−1.8%	5.7%	11
Fujii and Imura [1] – 5 cm × 10 cm		5.0	up	(30) $\overline{Nu^*}$	5.0%	−0.4%	5.0%	10
Lloyd and Moran [4] – electrochemical		2200	up	(30) $\overline{Nu^*}$	4.9%	+0.7%	4.8%	39
Churchill and Chu [5] – Cheesewright		0.70	vertical	(55) $\overline{Nu'}$	16.4%	−15.4%	5.6%	6
Churchill and Chu [5] – King		0.70	vertical	(55) $\overline{Nu'}$	13.5%	+11.1%	7.6%	8
Churchill and Chu [5] – Saunders		0.024	vertical	(55) $\overline{Nu'}$	5.3%	−1.2%	5.1%	18
Fujii and Imura [1] – 5 cm × 10 cm		5.0	vertical	(67) $\overline{Nu'}_w$	5.2%	+5.0%	1.6%	6
Churchill and Chu [5] – Jakob		0.70	vertical	(55) $\overline{Nu'}$	4.7%	+3.1%	3.5%	5
Hassani and Hollands [9] – 82 mm		0.71	vertical disk	(55) $\overline{Nu'}$	3.8%	−3.4%	1.6%	26
Kobus and Wedekind [9] – three sizes		0.71	vertical disk	(55) $\overline{Nu'}$	3.2%	−0.4%	3.1%	19
Fujii and Imura [1] – 30 cm × 15 cm		5.0	vertical	(67) $\overline{Nu'}_w$	2.2%	−0.5%	2.2%	5
Fujii and Imura [1] – 5 cm × 10 cm		5.0	down	(56) $\overline{Nu}_R$	4.2%	−3.4%	2.5%	15
Aihara et al. [3] – 25 cm × 35 cm		0.71	down	(56) $\overline{Nu}_R$	3.8%	−3.7%	0.9%	2
Faw and Dullforce [10] – 18.1 cm disk		0.71	down	(56) $\overline{Nu}_R$	3.7%	+1.8%	3.2%	3
Fujii and Imura [1] – 30 cm × 15 cm		5.0	down	(56) $\overline{Nu}_R$	2.7%	−0.8%	2.6%	8
Fujii and Imura [1] – 5 cm × 10 cm		5.0	inclined	(75, 77) $\overline{h}$	5.8%	−2.4%	5.3%	15
Fujii and Imura [1] – 30 cm × 15 cm		5.0	inclined	(75, 76) $\overline{h}$	3.3%	−2.2%	2.6%	14

Table 13 summarizes statistics for the eighteen data-sets presented in Figures 4, 6, 7, 8, 9, 10, 11, and their associated tables. They are grouped by orientation and ordered by decreasing error relative to the present work, All but three of these data-sets have RMSRE of 6% or less, quantitatively supporting the present theory for horizontal, vertical, and inclined plates.

25. Discussion

Rennó and Ingersoll [12] and Goody [13] found that the heat-engine efficiency limit for atmospheric convection is 1/2 of the reversible heat-engine efficiency limit η. This investigation finds that $\eta/2$ is the limit for external natural convection generally. Reversible heat engines, such as Stirling engines, can be more efficient than $\eta/2$. External convection is not reversible.

25.1 **Side-Walls.** The Fujii and Imura [1] side-walled plates do not qualify as external because fluid was not free to flow horizontally near the plate. The side-wall formulas are not general, particularly for square plates. They were investigated primarily to gauge how well the combination of ℓ^p-norm with trigonometric scaling of Ra explains heat transfer from inclined plates.

25.2 **Laminar Turbulent Transition.** Evidence from Lloyd and Moran [4], and statements in Fujii and Imura [1] and Churchill and Chu [5], that the laminar-turbulent transition was irrelevant to natural convection heat transfer were published in the early 1970s. Yet, belief that it governs external plate natural convection heat transfer has persisted [11, 18, 2].

Much of the subsequent natural convection literature investigates local flow properties. Such studies do not inform this investigation's systemic-invariant analysis. However, streamlines photographs were crucial to characterizing the flow topologies and deriving the present formulas.

25.3 **Pause in Horizontal Flow.** The pause in horizontal flow above the upward-facing 5 cm plate is visible in the $\theta = -90°$ photograph from Fujii and Imura [1]. Their photographs of vertical and downward-facing plate streamlines do not include enough of the fluid above the plates to see the horizontal pause expected by this investigation.

25.4 **Harmonic Mean.** The harmonic mean integral in Formulas (57) and (61) converges only when the perimeter curve is perpendicular to the integration axis at both integration limits. For downward-facing plates this includes all circles, ellipses, and rectangles; for vertical plates this includes all circles and ellipses, and trapezoids (including rectangles) with two vertical edges. When $\sqrt[3]{Ra'} \gg 1$, vertical plate $\overline{Nu'}$ scales with L'. Hence, the heat flow rate $\overline{h'} = k\,\overline{Nu'}/L'$ is sensitive to L' only at small Ra' values.

26. **Conclusions**

Using a novel methodology based on streamline photographs, dimensional analysis, and the thermodynamic constraints on heat-engine efficiency, this investigation:

- derived from first principles a previously unknown comprehensive heat transfer formula for upward-facing convection;
- extended the scope of vertical and downward-facing formulas from rectangles to other shapes with convex perimeters using the harmonic mean for the characteristic length metric; and
- unified the Pr dependence of vertical and downward-facing plates.

A comprehensive, exact model for natural convection from an external, isothermal flat surface can now be succinctly stated. For horizontal upward-facing plates:

$$\overline{Nu^*}(Ra^*) = Nu_0^* \left\| 1 - \frac{1}{\sqrt{8}} \;,\; \frac{{Nu_0^*}^{1/3}}{4} \sqrt[3]{Ra^*} \right\|_{1/2} \qquad Ra^* > 1$$

$$\left\| F_0 \;,\; F_1 \right\|_p = \left(|F_0|^p + |F_1|^p\right)^{1/p} \qquad Nu_0^* = \frac{2}{\pi} \approx 0.637$$

For vertical and downward-facing plates, the convection reduction due to self-obstruction is the Ra scaling factor $1/\,\Xi(Pr)$, yielding comprehensive formulas for vertical $\overline{Nu'}$ and downward $\overline{Nu}_R$:

$$\overline{Nu'}(Ra') = \left\| \frac{Nu_0'}{2} \;,\; \frac{{Nu_0'}^{4/3}}{8\sqrt[3]{2}} \left[\frac{Ra'}{\Xi(Pr)}\right]^{1/3} \right\|_{1/2} \qquad Ra' > 1$$

$$\overline{Nu}_R(Ra_R) = \frac{Nu_0'}{4} + \frac{{Nu_0'}^{6/5}}{2^{7/5}} \left[\frac{Ra_R}{\Xi(Pr)}\right]^{1/5} \qquad Ra_R > 1$$

$$\Xi(Pr) = \left\| 1 \;,\; \frac{0.5}{Pr} \right\|_{\sqrt{1/3}} \qquad Nu_0' = \frac{8^{5/4}}{\pi^2} \approx 1.363$$

The reduction in effective gravitational acceleration g also scales Ra. The average convective surface conductance for an external, isothermal plate inclined at angle θ from vertical is:

$$\overline{h} = k \begin{cases} \max\left(\overline{Nu'}(|\cos\theta|\; Ra')/L', \overline{Nu^*}\left(|\sin\theta|\; Ra'\; [L^*/L']^3\right)/L^*\right) & Ra' \sin\theta < -[L^*/L']^3 \\ \max\left(\overline{Nu'}(|\cos\theta|\; Ra')/L', \overline{Nu}_R\left(|\sin\theta|\; Ra'\; [L_R/L']^3\right)/L_R\right) & Ra' \sin\theta > [L_R/L']^3 \\ \overline{Nu'}\left(|\cos\theta|\; Ra'\right)/L' & \text{otherwise.} \end{cases}$$

- The upward-facing characteristic length L^* is the area-to-perimeter ratio.
- The vertical characteristic length L' is the harmonic mean of the perimeter vertical spans.
- The downward-facing characteristic length L_R is the harmonic mean of the perimeter distances to that bisector which is perpendicular to the shortest bisector.
- Ra' is the Rayleigh number computed with vertical characteristic length L'.

The harmonic mean metrics extend vertical $\overline{Nu'}$ and downward-facing $\overline{Nu}_R$ to non-rectangular plates.

The present theory was compared with eighteen data-sets from seven peer-reviewed articles, testing circular, rectangular, and inclined rectangular plates, laminar and turbulent flows, with $0.024 < Pr < 2200$ and $1 < Ra < 10^{12}$. All except three of the data-sets had between 2% and 6% RMSRE from the present theory.

- The $\overline{Nu^*}$ formula improves accuracy and Ra range substantially over the piece-wise power-laws currently employed for predicting upward convection heat transfer.
- With less than 1% difference between $\overline{Nu'}$ and the Churchill and Chu (1975) vertical formula, there is little need to replace it in existing applications.
- However, the published Schulenberg (1985) formula can return values which are 10% smaller than $\overline{Nu}_R$; $\overline{Nu}_R$ should replace it.

27. Nomenclature

A	plate area (m^2)
c_p	fluid specific heat at constant pressure ($\mathrm{J/(kg \cdot K)}$)
B	sum of mean lengths of plate parallel flows divided by L
C	plate area fraction responsible for flow induced heat transfer
D	effective length of heat transfer contact with plate divided by L
E	count of 90° changes in direction of fluid flow
g	gravitational acceleration ($\mathrm{m/s^2}$)
$\overline{h}$	average convective surface conductance ($\mathrm{W/(m^2 \cdot K)}$)
I	power flux ($\mathrm{W/m^2}$)
k	fluid thermal conductivity ($\mathrm{W/(m \cdot K)}$)
L	characteristic length (m)
M	air molar mass (kg)
$\overline{Nu}$	average Nusselt number
P	air pressure ($\mathrm{N/m^2}$)
Pr	Prandtl number
q	conduction power (W)
q^*_{SS}	dimensionless conduction shape factor
R	disk radius (m)
$\overline{R}$	universal gas constant ($\mathrm{J/(kg \cdot K)}$)
Ra	Rayleigh number
Re	Reynolds number
Sc	Schmidt number
S	conduction shape factor (m)
T	temperature (K)
u	fluid velocity (m/s)
V	air volume ($\mathrm{m^3}$)
W	work (J)
w	distance between side-walls (m)
$y_+,\ y_-$	perimeter functions (m)
$\overline{y}$	Harmonic mean of perimeter functions (m)
Greek Symbols	
α	fluid thermal diffusivity $= k/[\rho\, c_p]$ ($\mathrm{m^2/s}$)
β	fluid thermal expansion coefficient ($\mathrm{K^{-1}}$)
ΔQ	heat energy (J)
ΔT	temperature difference $= T - T_\infty$ (K)
η	thermodynamic heat-engine efficiency
ν	fluid kinematic viscosity ($\mathrm{m^2/s}$)
Π	dimensionless variable group
Φ	power flux ($\mathrm{W/m^2}$)
ρ	fluid density ($\mathrm{kg/m^3}$)
θ	surface angle from vertical ($-90°$ is face up)
Ξ	Ra self-obstruction (reciprocal) factor
Superscripts	
$*$	upward-facing plate
$'$	vertical plate
Subscripts	
0	conduction
$\forall$	unified
A	atmospheric natural convective
h	heated
i	induced flow along plate
k	kinetic

N	natural convective
p	plate
R	downward-facing plate
r	downward-facing disk
S	dimensionless shape factor
t	ideal turbine
w	with side-walls
∞	bulk fluid
?	possibly misprinted formula

Acknowledgments

Thanks to Dave Custer, Rich Hilliard, Roberta Jaffer, and anonymous reviewers for their useful suggestions.

28. References

[1] Tetsu Fujii and Hideaki Imura. Natural-convection heat transfer from a plate with arbitrary inclination. *International Journal of Heat and Mass Transfer*, 15(4):755–764, 1972, doi:10.1016/0017-9310(72)90118-4.

[2] K. Kitamura, A. Mitsuishi, T. Suzuki, and F. Kimura. Fluid flow and heat transfer of natural convection adjacent to upward-facing, rectangular plates of arbitrary aspect ratios. *International Journal of Heat and Mass Transfer*, 89:320–332, 2015, doi:10.1016/j.ijheatmasstransfer.2015.05.075.

[3] T Aihara, Y Yamada, and S Endö. Free convection along the downward-facing surface of a heated horizontal plate. *International Journal of Heat and Mass Transfer*, 15(12):2535 – 2549, 1972, doi:10.1016/0017-9310(72)90145-7.

[4] JR Lloyd and WR Moran. Natural convection adjacent to horizontal surface of various planforms. *Journal of Heat Transfer*, 96(4):443–447, 1974, doi:10.1115/1.3450224.

[5] Stuart W Churchill and Humbert HS Chu. Correlating equations for laminar and turbulent free convection from a vertical plate. *International journal of heat and mass transfer*, 18(11):1323–1329, 1975, doi:10.1016/0017-9310(75)90243-4.

[6] S. W. Churchill and R. Usagi. A general expression for the correlation of rates of transfer and other phenomena. *AIChE Journal*, 18(6):1121–1128, 1972, doi:10.1002/aic.690180606.

[7] J. H. Lienhard, IV and J. H. Lienhard, V. *A Heat Transfer Textbook*. Phlogiston Press, Cambridge, MA, 5th edition, August 2020. Version 5.10.

[8] R.J. Goldstein, E.M. Sparrow, and D.C. Jones. Natural convection mass transfer adjacent to horizontal plates. *International Journal of Heat and Mass Transfer*, 16(5):1025 – 1035, 1973, doi:10.1016/0017-9310(73)90041-0.

[9] C.J. Kobus and G.L. Wedekind. An experimental investigation into forced, natural and combined forced and natural convective heat transfer from stationary isothermal circular disks. *International Journal of Heat and Mass Transfer*, 38(18):3329 – 3339, 1995, doi:10.1016/0017-9310(95)00096-R.

[10] R.E. Faw and T.A. Dullforce. Holographic interferometry measurement of convective heat transport beneath a heated horizontal circular plate in air. *International Journal of Heat and Mass Transfer*, 25(8):1157 – 1166, 1982, doi:10.1016/0017-9310(82)90210-1.

[11] R. J. Goldstein and Kei-Shun Lau. Laminar natural convection from a horizontal plate and the influence of plate-edge extensions. *Journal of Fluid Mechanics*, 129:5575, 1983, doi:10.1017/S0022112083000646.

[12] Nilton Rennó and Andrew Ingersoll. Natural convection as a heat engine: A theory for cape. *J. Atmos. Sci.*, 53:572–585, 01 1995, doi:10.1175/1520-0469(1996)053¡0572:NCAAHE¿2.0.CO;2.

[13] Richard Goody. On the mechanical efficiency of deep, tropical convection. *Journal of the Atmospheric Sciences*, 60(22):2827–2832, 2003, doi:10.1175/1520-0469(2003)060¡2827:OTMEOD¿2.0.CO;2.

[14] T. Schulenberg. Natural convection heat transfer below downward facing horizontal surfaces. *International Journal of Heat and Mass Transfer*, 28(2):467 – 477, 1985, doi:10.1016/0017-9310(85)90080-8.

[15] E. Fermi. *Thermodynamics*. Dover books in physics and mathematical physics. Dover Publications, 1956.

[16] F.P. Incropera, D.P. DeWitt, T.L. Bergman, and A.S. Lavine. *Fundamentals of Heat and Mass Transfer*. Wiley, Hoboken, NJ, USA, 2007.

[17] H. T. Lin, W. S. Yu, and C. C. Chen. Comprehensive correlations for laminar mixed convection on vertical and horizontal flat plates. *Heat and Mass Transfer*, 25(3):353–359, Dec 1990, doi:10.1007/BF01811559.

[18] W.M. Rohsenow, J.P. Hartnett, and Y.I. Cho. *Handbook of heat transfer*. McGraw-Hill handbooks. McGraw-Hill, 1998.